MATERIAL PROPERTIES FROM MINIATURE PUNCH TEST AND FINITE ELEMENT ANALYSIS

MATERIAL PROPERTIES FROM MINIATURE PUNCH TEST AND FINITE ELEMENT ANALYSIS

By

DANIEL Y. DAI, B. ENG.

A Thesis

Submitted to the School of Graduate Studies

In Partial Fulfillment of the Requirements

for the Degree

Master of Applied Science

McMaster University

MASTER OF APPLIED SCIENCE
(Mechanical Engineering)

McMaster University
Hamilton, Ontario

TILTE: Material Properties from Miniature Punch Test and Finite Element Analysis

AUTHOR: Daniel Y. Dai, B. Eng.
(Jilin University of Technology)

SUPERVISOR: Dr. Don R. Metzger

NUMBER OF PAGES: x, 109

ABSTRACT

The Punch test provides a technique for the determination of material properties from small specimens. Using the rectangular specimen, the test can be used to control the orientation of the cracking plane which was not possible in the ball punch on a circular disk design. A three dimensional quarter finite element model was formulated to simulate the punch test for 150 °C and 300 °C tests performed on So8 steel. The comparison of predicted and measured load-deflection and stress-strain curves showed good agreement between FE model and tests. A user interface, which allows for routine application, with the necessary postprocessing capabilities was developed and tested for the purpose of simulating miniature punch tests and estimating stress-strain data from measured load curves.

ACKNOWLEDGEMENT

I would like to express my sincere gratitude to Dr. Don R. Metzger for his continual support and guidance throughout this research. I want to thank him for the opportunity and his kindly encouragement throughout the study. I would like to thank all my family for all the support they gave without a moments thought throughout my life. I would also like to thank my colleagues Young-Suk Kim, Li Pan and Yi-Hai Shi for their kindly support at various stages.

TABLE OF CONTENTS

LIST OF FIGURES

CHAPTER 1

INTRODUTION

1.1 Introduction to the Small Specimen Punch Test

A fundamental requirement in residual life assessment of a component in service is the determination of the material properties. Although a wide range of standard tests exists for the determination of material properties, the majority of these require large specimens. While it is possible to obtain such specimens during the manufacture of an engineering component, it is difficult, if not impossible, to obtain such a quantity of material from a component in service without degrading the integrity [1].

The punch test provides a technique for the determination of material properties from small specimens. This technique has been investigated by many workers for a number of years. In 1981, Manahan *et al.* [2] proposed a small punch test which was based on the determination of the force-displacement curve for a small flat-disc specimen when a central load was applied. Deformation of the disc was modeled with a finite element code. The results of these analyses were useful in identifying the various deformation regimes. An attempt was made to use the finite element method to find a

predicted load-displacement curve that matched the experimental one, however difficulties were encountered in identifying unique solutions.

Baik *et al.* [3] developed a technique to obtain fracture and impact data from punch tests, whereby small ferritic coupon specimens were clamped between two dies and deformed by penetrators with various tip geometries over a range of temperatures. The optimum tip geometry was identified as a 2.4-mm-diameter ball, and this test has subsequently been referred to as a "small punch" (SP) test.

Hemispherical-punch stretching tests have been conducted to evaluate the basic formability of sheet metals. Various three-dimensional finite element simulations for hemispherical-punch stretching have been presented as numerical analysis. Toh *et al.* [4] presented a procedure to construct the Forming Limit Curve (FLC) of sheet material using the FE simulation of the Hasek test [5], which were performed using hemispherical punch stretching of a circular blank with various circular cutoffs and various friction conditions at the tool-sheet interface. Yoshida *et al.* [6] also investigated the effects of material properties on strain distribution and histories of the deformation processes using three-dimensional FE program. Yoon *et al.* [7] presented numerical solutions of axisymmetric sheet stretching employing an experimentally determined stress-strain curve and measured overall coefficient of friction along the punch-sheet interface. Predicted values of loads, deflections, strain distributions and other relevant data are favorably compared with experimental values of these same quantities.

More recently, Brookfield *et al.* [1] have investigated the relationship between the specimen yield stress and the maximum punch force for an elastic-perfectly plastic material using the small disc punch test and finite element analysis. The effect of experimental artifacts on the punch force has been investigated through finite element analysis and physical experiment too.

Most of the small punch tests were designed as a ball punch on a circular disk, which were not applicable to anisotropic material. Based on a small ball-punch-on-rectangular-specimen concept, Lee *et al.* [12] developed a new punch test design. This new design, which provides a higher level of constraint in one direction, would force the fracture plane occur along a desired orientation. Using the finite element analysis and experimental test, this new punch design has been successfully applied to measurement of tensile behavior, Ductile-Brittle Transition Temperature (DBTT), and fracture toughness.

1.2 Finite Element Method

The finite element method is a numerical analysis technique for obtaining approximate solutions to a wide variety of engineering problems. Although originally developed to study stresses in complex airframe structures, it has since been extended and applied to the broad field of continuum mechanics. Because of its diversity and flexibility as an analysis tool, it is receiving much attention in industry [8].

The basic concept of the finite element method is to approximate a solution region by replacing it with an assemblage of discrete elements. The finite element discretization procedures must be applied to divide the solution region into elements and express the unknown field variable in terms of assumed approximating functions within each element.

There are basically three different approaches to formulate the properties of individual elements:

1. The direct approach which is traceable to the direct stiffness method of structural analysis and can be used only for relatively simple problems.

2. The variational approach which relies on the calculus of variations and must involve a functional which implicitly contains differential equations that describe the problem. This can be employed for both simple and sophisticated element shapes.

3. The weighted residuals approach which begins with the governing equations of the problem and proceeds without relying on a variational statement. This approach is widely used to derive element properties since it extend the finite element method to problems where no functional is available.

In general, the solution of a continuum problem by the finite element method follows an orderly step-by-step process [8], which can be summarized as:

1. Discretize the continuum. This is to divide the continuum or solution region into elements.

2. Select interpolation functions. This step is to assign nodes to each element and then choose the interpolation function to represent the variation of the field variable over the element.

3. Find the element properties. At this step, one of the three approaches is used to determine the matrix equations expressing the properties of the individual elements.

4. Assemble the element properties to obtain the system equations.

5. Impose the boundary conditions.

6. Solve the system equations. A set of simultaneous equations obtained from the assembly process is solved to obtain the unknown nodal values of the problem at this step.

7. Make additional computations if desired. Some other important parameters can be calculated from the solution of the system equations at this step.

1.3 Empirical Equations to Stress-Strain Curves

In order to determine the material properties in the small punch test, it is necessary to idealize the stress-strain behavior of the material (Fig. 1.1d). The empirical equations for the stress-strain curves can be used as the idealized model for the punch test:

1. Ludwik Power Law Expression

The Ludwik expression [9] is one of the most common methods of approximately representing the true stress-strain curve. It is expressed in the form

$$\sigma = \sigma_y + H\varepsilon^n \tag{1-1}$$

where σ_y is the initial yield stress, H is a constant strain hardening rate, and n is a strain-hardening exponent, $0 \le n \le 1$.

There are two cases for this equation:

(i) $n = 1$, shown in Figure 1.1a. The equation represents a rigid linear work-hardening material which is rigid up to the yield stress σ_y, followed by deformation at a constant strain hardening rate H.

(ii) $0 < n < 1$, shown in Figure 1.1b. This expression is applicable when the material is work hardening and the elastic strains may be safely neglected in an analysis. The higher the value of strain-hardening exponent n, the more pronounced is the strain-hardening characteristic of the material. When

$\sigma_y = 0$, the curves are as given in Figure 1.1c. This expression should not be used for small strains since $d\sigma / d\varepsilon$ for $n \neq 1$ is infinite at $\varepsilon = 0$.

2. Ramberg-Osgood Expression

Another frequently used form due to Ramberg and Osgood [10] may be expressed as

$$\varepsilon = \frac{\sigma}{E}\left\{1 + \alpha\left(\frac{\sigma}{\sigma_0}\right)^{m-1}\right\} \tag{1-2}$$

where σ_0 is a nominal yield stress, α and m are dimensionless constant, $m \geq 1$. It gives a nonlinear stress-strain curve shown in Fig. 1.2. The initial slope of the curve takes the value of Young's modulus E at $\sigma = 0$, and decreases monotonically with increasing loading. For a nonhardening material ($m = \infty$), the equation degenerates into a pair of straight lines meeting at the yield point $\sigma = \sigma_0$. This expression allows for a better fit of real stress-strain curves since three parameters are involved.

3. Another common method is to use bilinear or multi linear expressions between stress and strain. This is illustrated in Figure 1.3, where $\sigma = E\varepsilon$ for elastic part (from 0 to σ_y) and $\sigma = P\varepsilon$ for plastic part (above σ_y). E may be interpreted as an elastic modulus and P as a plastic modulus.

1.4 Elastic-plastic Bending

In the punch test, the specimen is subjected to an external punch load of gradually increasing magnitude and plastic flow begins at a stage when the yield criterion is first satisfied in the most critically stressed element. Further increase in load causes spreading of the plastic zone which is separated from the elastic material. Since the load is applied steadily without shock and impact, the specimen of the punch test can be simplified to a pure beam bending model.

Fig. 1.4 shows the bending of the beam. A segment of a beam with rectangular cross section subjected to bending moments. The neutral axis coincides with the centroidal axis, as the cross section of the beam has two axes of symmetry and the stress-strain diagram is alike in tension and compression (Fig. 1.4 a). As progressively increasing bending moments are applied to the beam, the strains increases as shown in Fig 1.4 b. Corresponding to these strains and their linear variation from the neutral axis, the stress distribution looks as shown in Fig 1.4 c.

Since the beam acts in pure bending, the static equations can be used in establishing the flexure formula. The bending moment at any stage is given by

$$M = -\int_A \sigma(\varepsilon) y dA \tag{1-3}$$

where σ is the normal stress acting on an infinitesimal element of the cross-sectional area A of the beam, for work hardening material σ is the function of strain ε, and y is the distance from the neutral axis to an element dA.

With the assumption of pure bending, the strain energy of the specimen due to the deflection is equal to the work of the bending moment, therefore is equal to the work of external punch load. The stress-strain relations then can be determined based on this conservation of energy. Pure bending is also useful to test the methodology of finding the material properties because the strain distribution is single and sensitivity is similar to the punch test.

1.5 Thesis Objective

The objective of the thesis is to evaluate a new technique for determination of material properties from the small specimen punch test, also to provide a capability for processing the simulation and test data such that expert knowledge of finite element modeling is not essential, and so that stress-strain curves could be efficiently obtained.

The objective will be met by creating a dedicated finite element model with a user interface such that only specific inputs would be required. The model will use the existing H3DMAP finite element program. The parameters of the FE simulation will be determined following the experimental procedures as closely as possible. The interface with the necessary post-processing capabilities would be developed and tested to

establish its validity for the intended purpose of simulating miniature punch tests and estimating stress-strain data from measured load curves. This would allow for routine application of the program to punch test data without expert knowledge of the finite element method.

1.6 Thesis Outline

The thesis begins with the introduction of the small punch test and finite element methods. The elastic-plastic bending model of the punch test is interpreted. Different empirical equations to stress-strain curves are discussed.

Chapter two elaborates the finite element method for the punch test. The governing equations are introduced first. The weak form of the equation of motion is developed. The constitutive model of the punch test is then interpreted. The explicit direct integration methods which were used in the finite element analysis for the punch test are discussed at the end of this chapter.

The methodology of the material properties determination is developed in chapter three. The balance of the energy, which includes punch work, internal strain energy and clamping energy, was interpreted afterwards.

In chapter four, the experimental method of the small punch test and finite element modeling are discussed at the beginning. The FE model is validated by comparison with

experimental data. The analysis procedures and sensitivity to experimental parameters are discussed. The FORTRAN program implementation is developed at the end of this chapter. The testing results of two types of specimens are demonstrated and discussed in chapter five.

Finally in chapter six, the conclusions of the work are summarized along with the suggestions for the future work.

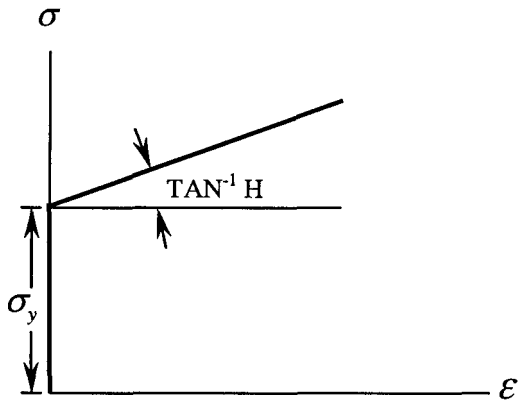

(a) Rigid linear work hardening

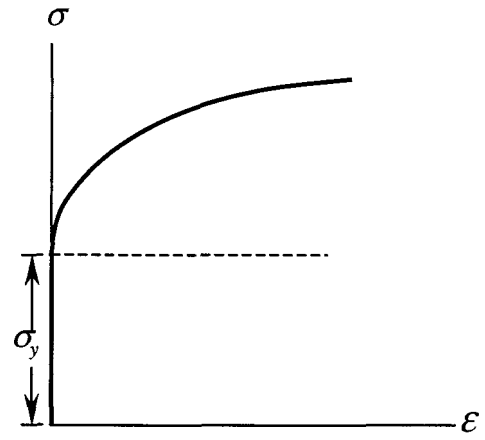

(b) Rigid nonlinear work hardening

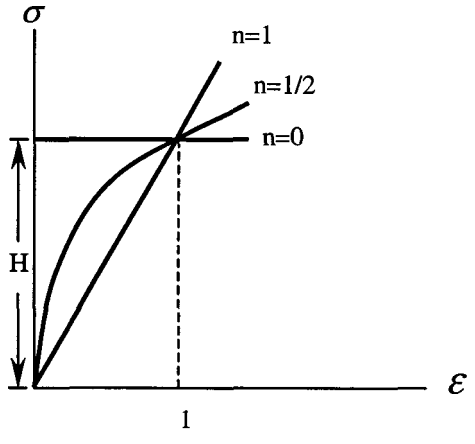

(c) Empirical curves for $\sigma = H\varepsilon^n$

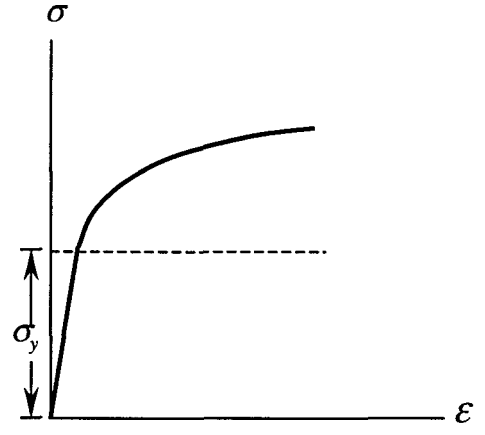

(d) Stress-strain curve

Figure 1.1 Ludwik's empirical equation.

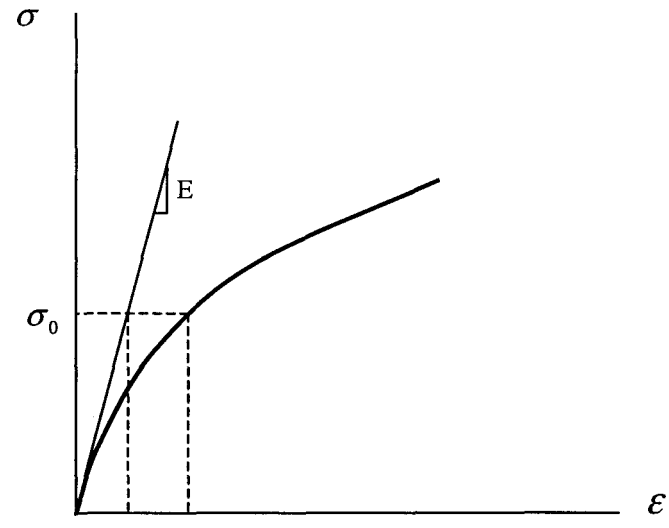

Figure 1.2 Empirical curve for Ramberg-Osgood expression.

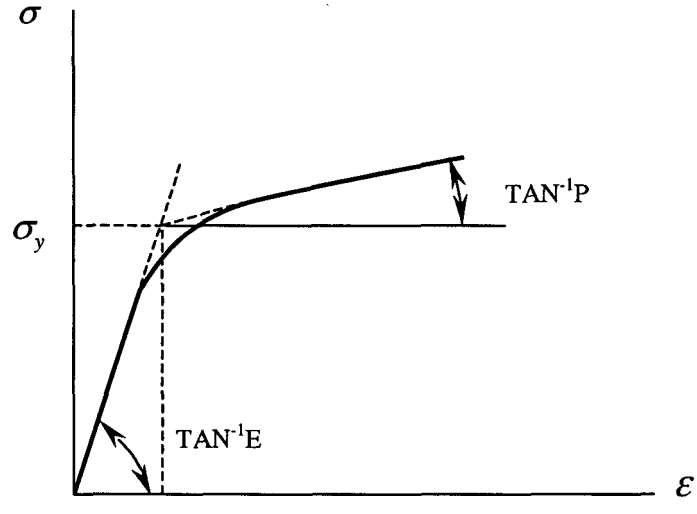

Figure 1.3 Approximating bilinear stress-strain curve.

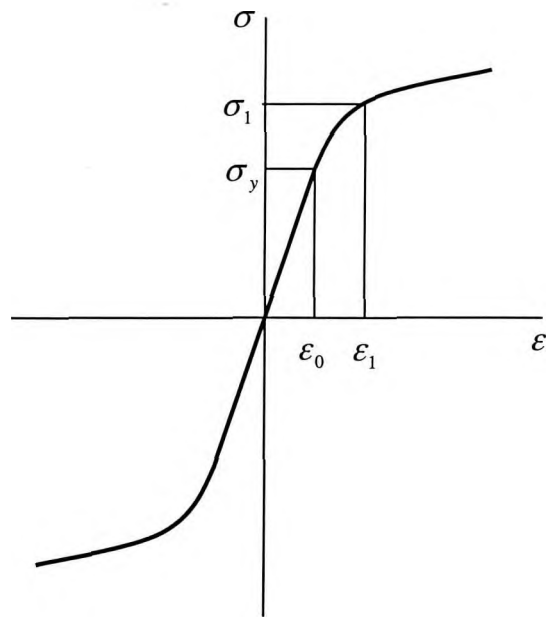

(a) Stress-strain diagram

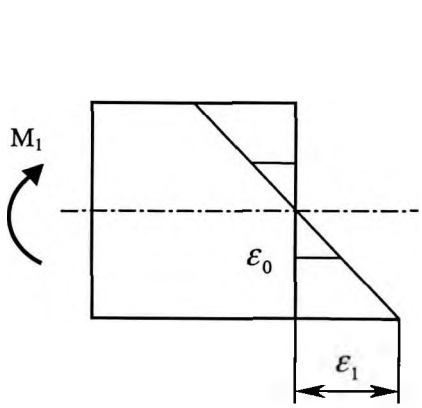

(b) Strain distribution

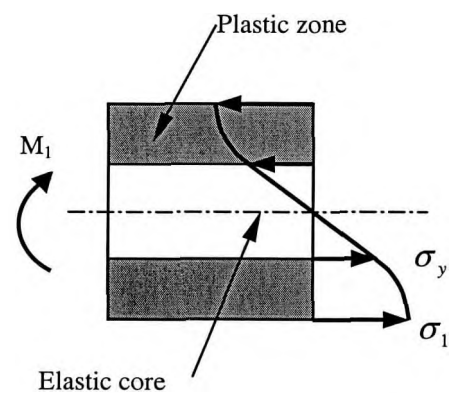

(c) Stress distribution

Figure 1.4 Elastic-plastic beam bending.

CHAPTER 2

FINITE ELEMENT METHOD FOR THE PUNCH TEST

In order to determine the material properties from the punch test, the finite element analysis is undertaken. In the simulation of the small punch test, the mathematical formulations of contact and impact problems are developed. All of the formulations developed in a general form to suit for all the three dimensional problems. Since the specimen material model is elastic-plastic model, the nonlinearity is involved. The H3DMAP finite element code is imposed for the punch test analysis, this code provides an explicit integration method which gives the efficient and accurate solution to large-scale problems with nonlinearity.

2.1 Governing Equations

The behavior of continuum generally is governed by three major groups of equations, i.e. the equation of motion, constitutive equations, and initial conditions and boundary conditions.

2.1.1 Strain Measure

The strain measure gives the strain-displacement relation which is a key ingredient in the formulation of finite elements for stress analysis problems. Since large deformation is involved in the finite element simulation, the rate-of-deformation strain measure is used, the tensor equation can be given as follows:

$$D_{ij} = \frac{1}{2}\left(\dot{u}_{i,j} + \dot{u}_{j,i}\right) \tag{2.1-1}$$

where the comma indicates partial differentiation with respect to x_j or x_i, i.e. $u_{i,j} = \partial \dot{u}_i / \partial x_j$, $u_{j,i} = \partial \dot{u}_j / \partial x_i$. If the strain rate is always based on updated geometry, its integration over time corresponds to logarithmic strain (also called true strain).

2.1.2 Stress Measure

A common stress measure is the Cauchy stress tensor, which gives the actual traction on an imaginary plane at a point within the body (Malvern 1969). The traction vector on an arbitrary plane at a point can be obtained as

$$q_i = \sigma_{ij} n_j \tag{2.1-2}$$

where n is a unit normal vector of the plane.

2.1.3 Kinetic Equilibrium

The Kinetic Equilibrium is also called equations of motion that obtained by using the momentum principles [17], which state that the time rate of change of the total momentum of a given set of particles equals the vector sum of all the external forces acting on the particles of the set. The equation of motion within the body can be written as

$$\frac{\partial \sigma_{ji}}{\partial x_j} + F_i = \rho \ddot{x}_i \tag{2.1-3}$$

where σ_{ij} is Cauchy stress component, $\ddot{x}_i$ is the acceleration component, i.e. $\ddot{x}_i = \partial^2(x_i)/\partial t^2$, F_i is the body force, ρ is the mass density of the material. Summation over repeated indices i and j (here i and j are determined from the value of 1, 2 and 3 corresponding to x, y and z directions respectively) are applied.

2.1.4 Constitutive Equations

Constitutive equations give the stress-strain relations of the material. For the elasto-plastic material, the incremental stress-strain relation is used in the elastic-plastic regime according to the plasticity theory.

The stress increments can be evaluated using

$$\{d\sigma\} = [E]\{d\varepsilon^e\} = [E](\{d\varepsilon\} - \{d\varepsilon^p\}) \tag{2.1-4}$$

where $\{d\sigma\}$ is the stress increment, $\{d\varepsilon\}$ is the total strain increment, $\{d\varepsilon^e\}$ and $\{d\varepsilon^p\}$ are the elastic and plastic strain increment respectively, and $[E]$ is the elastic stiffness matrix. According to the associated flow rule, which is commonly used for ductile metals, the plastic strain increments can be calculated from the function F,

$$\left\{d\varepsilon^p\right\} = \left\{\frac{\partial F}{\partial \sigma}\right\} d\lambda \tag{2.1-5}$$

where $d\lambda$ is a scalar, F is a yield function.

The yield criterion, which is a function of stresses $\{\sigma\}$, hardening parameter $\{\alpha\}$ and plastic work W_P can be expressed as

$$F(\sigma, \alpha, W_P) = 0 \tag{2.1-6}$$

To satisfy the constitutive law, for the material is in the elastic range or is yielding, results $dF \leq 0$ has been met. The mathematical expression can be given as

$$dF = \left\{\frac{\partial F}{\partial \sigma}\right\}^T \{d\sigma\} + \left\{\frac{\partial F}{\partial \alpha}\right\}^T \{d\alpha\} + \frac{\partial F}{\partial W_p} dW_p \tag{2.1-7}$$

Combining above equations, the stress increments can be evaluated using

$$\{d\sigma\} = [E_{ep}]\{d\varepsilon\} \tag{2.1-8}$$

where $[E_{ep}]$ can be regarded as a generalized form of tangent modulus. It must be noted that above stress-strain law depends on the yield function F used, and depending on the material characteristics to be modeled.

2.1.5 Boundary Conditions

Since the contact problem is involved in the punch test, the system must satisfy the traction and displacement boundary conditions, which are denote by Γ_F and Γ_D respectively.

$$\begin{aligned} n_j \sigma_{ij} &= \bar{q}_i \qquad \text{on } \Gamma_F \\ u_i &= \bar{u}_i \qquad \text{on } \Gamma_D \end{aligned} \tag{2.1-9}$$

where $\bar{u}_i$ and $\bar{q}_i$ are prescribed displacement components and boundary traction components respectively, and n_j are the components of an outward unit normal vector on the boundary Γ_F. The velocity and acceleration on Γ_D can also be prescribed from the displacement boundary condition:

$$\begin{aligned} \dot{u}_i &= d\bar{u}_i / dt \qquad \text{on } \Gamma_D \\ \ddot{u}_i &= d^2\bar{u}_i / dt^2 \qquad \text{on } \Gamma_D \end{aligned} \tag{2.1-10}$$

The condition of Eq. 2.1-9 must be used for all regions where motion or traction is imposed.

2.1.6 Initial Conditions

The initial conditions which are to be satisfied by the displacement field $u(x,t)$ can be simply expressed in terms of the displacements and velocities:

$$u(X,0) = \overline{u}(X)$$
$$\dot{u}(X,0) = \overline{\dot{u}}(X) \qquad (2.1\text{-}11)$$

where $\overline{u}(X)$ and $\overline{\dot{u}}(X)$ are the prescribed values for $u(X,0)$ and $\dot{u}(X,0)$, respectively. If the body is initially undeformed and at rest, the initial conditions can be written as

$$u(X,0) = 0$$
$$\dot{u}(X,0) = 0 \qquad (2.1\text{-}12)$$

In forming problems, initial condition usually correspond to a system at rest, $u = 0, \dot{u} = 0$.

2.1.7 Interior Continuity Conditions

For a pair of contacting bodies (Fig. 2.1) in equilibrium and in transient problems, the jump conditions must be met by the stresses along the contact discontinuity as

$$(\sigma_{ij}^{+} - \sigma_{ij}^{-})n_j = 0 \qquad (2.1\text{-}13)$$

where n_j denotes the normal vector of the contacting bodies, $\sigma_{ij}^{+}, \sigma_{ij}^{-}$ are the stress components on the contact area, and the superscripts "+" and "-" refer to the stresses on two sides of the contact discontinuity. In the punch test, this is needed for the contact surfaces between punch and specimen, and specimen and dies.

2.2 Finite Element Discretization

The differential equations and the boundary conditions, which are defined in previous section, are called the strong form. The analytical solution for strong form rarely can be achieved in the punch test system due to the complex geometric configuration and contacting constraints. A weak form, which is an integral expression that implicitly contains the differential equations and the boundary conditions, provides the possibility to solve such problems. In order to find the weak form of the problem, the finite element discretization is needed.

The weak form can be developed typically in two ways, one is the variational formulation (Rayleigh-Ritz method) which is based on the principle of stationary potential energy. The other one is the method of weighted residuals.

In some cases, the variational principle may be unobtainable. The weighted residual method can be applied to construct an approximate solution of differential equations for

the problem. The Galerkin method, which is the most popular weighted residual method, uses integral expressions that contain the differential equations of a physical problem.

2.2.1 Weighted Residual Methods

For an arbitrary physical problem, the governing differential equations and boundary conditions can be symbolized as

$$\begin{aligned} Du - f &= 0 \qquad \text{in domain } V \\ Bu - g &= 0 \qquad \text{on boundary } S \text{ of } V \end{aligned} \tag{2.2-1}$$

If the exact solution $u = u(x)$ of Eq. 2.2-1 is difficult to determine, an approximate solution $\tilde{u}$ is made instead. Typically $\tilde{u}$ interpolates as a polynomial that satisfies essential boundary conditions and contains undermined coefficients, $\tilde{u} = \tilde{u}(a,x)$. The discrepancy of the approximate solution can be expressed as residuals R_D and R_B, which are functions of x and the a_i:

$$\begin{aligned} R_D &= R_D(a,x) = D\tilde{u} - f \qquad \text{(interior residual)} \\ R_B &= R_B(a,x) = B\tilde{u} - g \qquad \text{(boundary residual)} \end{aligned} \tag{2.2-2}$$

Since $\tilde{u} = \tilde{u}(a,x)$ satisfies essential boundary conditions, only R_D is needed for the determination of $\tilde{u}$.

Residuals may vanish for some values of x, but they are not zero for all x unless $\tilde{u}$ is the exact solution. If residuals are small enough, the approximate solution $\tilde{u}$ can be used to instead the exact solution u. To minimize the residual the Galerkin method is applied, which uses a weight function and set the weighted averages of residual R_D to zero,

$$R_i = \int_V W_i(x) R_D(a, x)\, dV = 0 \qquad (2.2\text{-}3)$$

where W_i is the weight function, $W_i = \partial\tilde{u} / \partial a_i$

2.2.2 Galerkin Method Implementation

Based on the momentum equation (Eq. 2.1-3), the boundary (Eq. 2.1-7) and interior continuity (Eq. 2.1-11) conditions, the Galerkin residual equation for a single element in the weak form can be expressed as

$$R = R_V + R_S = 0$$

$$= \int_V W_i \left(\frac{\partial \bar{\sigma}_{ji}}{\partial x_j} + \rho F_i - \rho \ddot{\bar{x}}_i \right) dV + \int_S W_i \left(n_j \bar{\sigma}_{ji} - t_i \right) dS + \int_S W_i \left(n_i^A \bar{\sigma}_{ij}^A + n_i^B \bar{\sigma}_{ij}^B \right) dS \qquad (2.2\text{-}4)$$

where W_i is the weigh function, $\bar{\sigma}_{ji}$ and $\ddot{\bar{x}}_i$ are the approximation function of the σ_{ji} and $\ddot{x}_i$ respectively. The weight function can be defined to be the same as the interpolation function in the acceleration fields:

$$\ddot{\bar{x}}_i = \sum_{j=1}^{n} N_j^k \ddot{x}_i^j \quad \text{and} \quad W_i = N_i \tag{2.2-5}$$

where N_i is the interpolation function.

From Gauss's theorem, the interior continuity conditions, and the traction boundary conditions, the discretized governing equation can be obtained as

$$\sum_{k=1}^{NE} \left[\int_{V_k} B^T \sigma \, dV - \int_{V_k} N^T F dV - \int_{S_k} N^T \bar{t} \, dS + \int_V \rho N^T N dV \, \ddot{x} \right] = 0 \tag{2.2-6}$$

For dynamic contact problem, it can be written in the alternative form

$$M \ddot{x} + F_{\text{int}}^t = F_{ext}^t \tag{2.2-7}$$

where the mass matrix are defined as

$$M = \sum_{k=1}^{NE} \left[\int_{V_k} \rho N^T N dV \right] \tag{2.2-8}$$

and the internal force and external load are defined as

$$F_{\text{int}}^t = \sum_{k=1}^{NE} \left[\int_{V_k} B^T \sigma \, dV \right] \tag{2.2-9}$$

$$F_{ext}^t = \sum_{k=1}^{NE} \left[\int_{V_k} N^T F dV + \int_{S_k} N^T \bar{t}_i dS \right] \tag{2.2-10}$$

Eq. 2.2-8 is called consistent mass matrix, since it is evaluated using the same shape functions as are used to generated the element stiffness matrix [26]. A simpler and historically earlier formulation is the lumped mass matrix, which is obtained by placing particle masses m_i at nodes i of an element, such that $\sum m_i$ is the total element mass [15]. Because of the diagonal property, the lumped mass matrix is often used in the explicit integration methods.

2.3 Constitutive Model

In the punch test, the plastic deformation of the specimen is involved. With plastic deformation, the stress-strain relation is no longer unique and will depend on the deformation history. To discuss the material model in the punch test, the followings are assumed: the material model is elasto-plastic model with isotropic hardening, the material response is rate-independent, the contact bodies undergo only small displacements and that frictional effects can be neglected.

2.3.1 Constitutive Relations for Elastic-plastic Materials

To describe the constitutive model of the specimen in the punch test, the well-known hardening curve, as shown in Figure 1.1d under uniaxial loading, is imposed. In this model, the material deforms elastically until the yield stress is reached. Beyond the yield

stress, plastic deformation occurs, and the material hardens as the plastic deformation increases.

The plastic deformation can be decomposed into two parts, the elastic part ε_{ij}^{e} and plastic part ε_{ij}^{p}. This can be expressed as

$$\varepsilon_{ij} = \varepsilon_{ij}^{e} + \varepsilon_{ij}^{p} \tag{2.3-1}$$

The increments in strain then can be expressed in the rate form

$$\dot{\varepsilon}_{ij} = \dot{\varepsilon}_{ij}^{e} + \dot{\varepsilon}_{ij}^{p} \tag{2.3-2}$$

where the dot denotes the time derivative of the associated quantity.

In the nonlinear elastic-plastic regime, the stress-strain relation is given by

$$\dot{\sigma} = E^{\tan}\dot{\varepsilon} \tag{2.3-3}$$

where the elastic-plastic tangent modulus, $E^{\tan}$, is the slope of the stress-strain curve.

The plastic strain rate is given by a flow rule which is often specified in terms of a plastic flow potential ϕ:

$$\dot{\varepsilon}_{ij}^{p} = \dot{\lambda}\frac{\partial \phi}{\partial \sigma_{ij}} \tag{2.3-4}$$

where $\dot{\lambda}$ is the plastic rate parameter.

The widely used von Mises yield criterion with an associative flow rule is used as the yield conditon:

$$\phi(\sigma,k)=\frac{1}{2}\tau_{ij}\tau_{ij}-\frac{1}{3}k^2=0 \tag{2.3-5}$$

where k is a state variable depending on the plastic deformation, τ_{ij} is the deviatoric stress.

2.3.2 Radial Return Algorithm

The integration process is needed for the stress calculation from the constitutive equations which characterize the analysis of elasto-plastic material. It is important to choose an appropriate integration procedure, since the integration of the elasto-plastic constitutive equations has significant influences on the accuracy and efficiency of the numerical solution procedure for contact problems with plastic deformation. The radial return method, which is used in this finite element analysis, is an effective and robust method.

The general process of radial return is: consider that at time step n in a loading sequence, from the previous solution step, ε_{ij}^n, $\varepsilon_{e\,ij}^n$, $\varepsilon_{P\,ij}^n$, σ_{ij}^n, and σ_{ys}^n are given, the

total strain increment, $\Delta\varepsilon_{ij}^{n}$ can be determined from the displacement increment Δu^{n}, and $\Delta\varepsilon_{e\,ij}^{n}$, $\Delta\varepsilon_{P\,ij}^{n}$, σ_{ij}^{n+1}, and σ_{ys}^{n+1} for time $n+1$ then can be computed from previous values. The algorithm of radial return is shown in Table 2.2.

2.4 Explicit Direct Integration Methods

Traditionally, the finite element method has been applied to steady-state problems using implicit methods. In the presence of complex geometry, nonlinear material behavior, large local material rotations, and large relative sliding of material interfaces, solutions using implicit methods may become intractable [11]. The explicit time integration makes possible the solution of large-scale problems, since it uses small time steps and avoids the linearization and Newton solver of the implicit methods.

2.4.1 Central Difference Method

The most widely used explicit method is the central difference method [26]. The central difference method is developed from central difference formulas which are obtained by expanding the Taylor series about time Δt. It approximates the velocity and acceleration (Fig. 2.3) by

$$\dot{x}^{t-\Delta t/2} = \frac{1}{\Delta t}(x^{t} - x^{t-\Delta t})$$

$$\ddot{x} = \frac{1}{\Delta t}(\dot{x}^{t+\Delta t/2} - \dot{x}^{t-\Delta t/2}) \tag{2.4-1}$$

This can be converted to an integration formula by rearranging the terms as follows:

$$\dot{x}^{t+\Delta t/2} = \dot{x}^{t-\Delta t/2} + \Delta t\ddot{x}^{t}$$

$$x^{t+\Delta t} = x^{t} + \Delta t\dot{x}^{t+\Delta t/2} \tag{2.4-2}$$

where Δt is a constant time increment.

For the undamped equation of motion, Eq. 2.1-3, the $\ddot{x}^{t}$ can be obtained

$$\ddot{x}^{t} = M^{-1}(F_{ext}^{t} - F_{\text{int}}^{t}) \tag{2.4-3}$$

where diagonal lumped mass M is used, to provide uncoupled equations and computational efficiency in this explicit integration. The computational procedures for central difference integration of undamped equations of motion are listed in Table 2.4.

2.4.2 Critical Time Step

The central difference method, like all explicit methods, is conditionally stable and requires Δt such that

$$\Delta t \leq \frac{2}{\omega_{\max}} \tag{2.4-4}$$

where $\omega_{\max}$ is the highest natural frequency of the system.

It is important to determine $\omega_{\max}$ to get the critical time step. If Δt is too large, the system is unstable, and if Δt is much smaller than necessary, computations are too expensive. The highest frequency of the element can be estimated as

$$\omega_{\max} = \frac{2C_D}{L_{\min}} \tag{2.4-5}$$

where C_D is the dilatational wave speed, and $L_{\min}$ is the minimum effective element length [15]. The critical time step Δt_{cr} is then obtained as

$$\Delta t_{cr} = \frac{L_{\min}}{C_D} \tag{2.4-6}$$

which is also called the CFL condition after Courant, Friedrichs, and Lewy [13] in finite difference methods.

2.4.3 Hybrid Explicit Solution

The punch test simulation involves complex geometry, large relative sliding contact surfaces and nonlinear material properties. The dynamic relaxation techniques [26,27] have distinct advantages over implicit methods in the solution of nonlinear problems involving large numbers of equations. Recently Sauve and Metzger [11] have demonstrated the efficient methods for steady state problems involving severe

nonlinearities, complex geometries and large relative sliding of material interfaces. Unfortunately, in this small punch test, the load keeps changing, so a static result will never be obtained. However since the loading rate is very slow, a hybrid explicit method [25] developed by Sauve and Metzger gives a numerical efficiency for this problem.

2.4.4 Hybrid Operator

The idea behind the hybrid operator is to combine the features of the explicit transient operator with those of dynamic relaxation which view the solution of a static problems as the steady state solution of a damped wave equation [25].

At time t, the equations of motion are givens as

$$M\ddot{x}^t + C\dot{x}^t + K(x^t)u^t = F_{ext}^t \tag{2.4-7}$$

Referring to the central difference expressions for acceleration and velocity Eq. 2.4-2, the average value of velocity is taken as

$$\dot{x}^t = \frac{\left(\dot{x}^{t+\Delta t/2} + \dot{x}^{t-\Delta t/2}\right)}{2} \tag{2.4-8}$$

Substituting into the equation of motion Eq. 2.4-7 yields

$$\frac{M}{\Delta t}(\dot{x}^{t+\Delta t/2} - \dot{x}^{t-\Delta t/2}) + \frac{C}{2}(\dot{x}^{t+\Delta t/2} + \dot{x}^{t-\Delta t/2}) + F_{\text{int}}^t = F_{ext}^t \tag{2.4-9}$$

Rearranging the terms, get

$$\dot{x}^{t+\Delta t/2} = \left(\frac{M}{\Delta t} + \frac{C}{2}\right)^{-1}\left[(F_{ext}^{t} - F_{\text{int}}^{t}) + \left(\frac{M}{\Delta t} - \frac{C}{2}\right)\dot{x}^{t-\Delta t/2}\right] \tag{2.4-10}$$

A diagonal mass matrix M along with a damping matrix C is used to maintain the efficiency and form of the central difference operator, and requires

$$C = c'M \tag{2.4-11}$$

where c' is damping factor based either mass proportional or displacement dependent damping.

Substituting for C in Eq. 2.4-10 yields

$$\dot{x}^{t+\Delta t/2} = \frac{[\Delta t M^{-1}(F_{ext}^{t} - F_{\text{int}}^{t}) + \dot{x}^{t-\Delta t/2}(1 - 0.5c'\Delta t)]}{(1 + 0.5c'\Delta t)} \tag{2.4-12}$$

The current coordinate $\dot{x}^{t+\Delta t}$ can be obtained from Eq. 2.4-2, and the current displacement vector $u^{t+\Delta t}$ is obtained as

$$u^{t+\Delta t} = u^{t} + \Delta t \dot{x}^{t+\Delta t/2} \tag{2.4-13}$$

By a judicious choice of c', Δt and M, the response can be attenuated resulting in the steady state solution to

$$F_{\text{int}} = F_{ext} \tag{2.4-14}$$

In order to maintain the stability of the explicit operator and to have reasonable estimates of the participating mode frequency for damping calculations, it is necessary to have an adaptive mass scheme; for a specified time Δt, the mass is obtained as

$$m_{ii} \geq 0.25\Delta t^2 \sum_{j=1}^{N} \left| K_{ij} \right| \tag{2.4-15}$$

where K is the current tangent stiffness matrix and N is the number of equations.
In the explicit solution, tangent stiffness, K, is not directly assembled, instead it is estimated from the system internal force vector F_{int}. This can be expressed as

$$K^t \approx \frac{[F_{\text{int}} - F_{\text{int}}^{t-\Delta t}]}{\Delta t \dot{x}^{t-\Delta t/2}} \tag{2.4-16}$$

The algorithm of the hybrid explicit solution in finite element code is summarized in Table 2.5.

2.4.5 Hourglass Stabilization

Explicit methods, which are used in the punch test simulation, rely on the economical evaluation of internal forces at each time step. One-point quadrature provides the greatest efficiency to minimize the number of operations per time step. However, the spurious hourglass deformation modes may occur with such formulations. The hourglass

mode is a deformation mode (not a rigid-body motion) but nevertheless produces zero strain energy. The hourglass control or hourglass stabilization therefore has to be applied to obtain useful results. For the finite element analysis in this study, the unified deviatoric hourglass control [21] is used.

In this chapter, the governing equations are discussed at the beginning. The weak form of the governing equations is then developed from the Galerkin method. The constitutive model of the specimen in the punch test is introduced. A hybrid explicit solution, which is used in the FE simulation, is discussed at the end of this chapter. This hybrid explicit method demonstrates the efficiency for the punch test which involves complex geometry, large relative sliding contact surfaces and nonlinear material properties. All of the topics of the finite element method discussed in this chapter are necessary for later analysis.

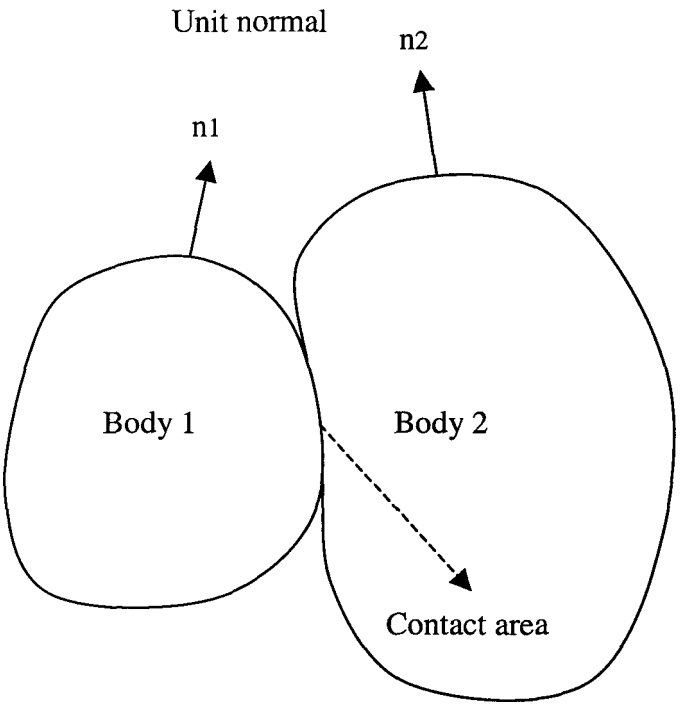

Figure 2.1 Model of contact bodies

1) Compute a deviatoric elastic trial stress as if no further plastic strain occurred

$$s_{ij}^{n+1} = \sigma_{ij}'^{n} + 2G\Delta\varepsilon_{ij}'^{n}, \qquad \text{where} \quad \sigma_{ij}' = \sigma_{ij} - \frac{1}{3}\delta_{ij}\sigma_{kk} = \sigma_{ij} - P\delta_{ij}$$

2) Compute the von Mises effective trial stress, which depends on deviatoric stress only

$$\bar{s}^{n+1} = \left(\frac{3}{2}s_{ij}^{n+1}s_{ij}^{n+1}\right)^{1/2}$$

3) Check yield function for plastic loading. If $\bar{s}^{n+1} > \sigma_{ys}^{n}$, then scale back stress to be at the yield surface:

$$\sigma_{ij}'^{n+1} = \left(\frac{\sigma_{ys}^{n+1}}{\bar{s}^{n+1}}\right)s_{ij}^{n+1}, \qquad \text{if} \qquad \bar{s}^{n+1} > \sigma_{ys}^{n}$$

$$\sigma_{ij}'^{n+1} = s_{ij}^{n+1}, \qquad \text{if} \qquad \bar{s}^{n+1} \le \sigma_{ys}^{n}$$

4) Determine effective plastic strain increment and new yield stress in terms of old quantities

$$\Delta\bar{\varepsilon}_{p}^{n} = \frac{\bar{s}^{n+1} - \sigma_{ys}^{n}}{3G + H}, \quad \sigma_{ys}^{n+1} = \sigma_{ys}^{n} + H\Delta\bar{\varepsilon}_{p}^{n}$$

5) Scale back elastic trial stress according to new yield stress

$$\sigma_{ij}'^{n+1} = \left(\frac{\sigma_{ys}^{n+1}}{\bar{s}^{n+1}}\right)s_{ij}^{n+1}$$

6) Add pressure to deviatoric stress to obtain the new total stress

$$P^{n+1} = P^{n} + \frac{E\Delta\varepsilon_{kk}^{n}}{3(1-2\nu)}, \quad \text{and} \quad \sigma_{ij}^{n+1} = \sigma_{ij}'^{n+1} + P^{n+1}\delta_{ij}$$

7) Repeat from step 1) until analysis is done.

Table 2.2 Radial return algorithm.

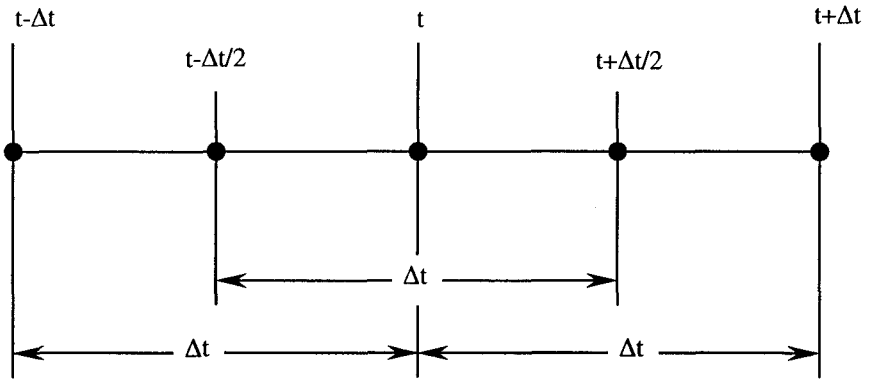

$$\dot{x}^{t+\Delta t/2} = \dot{x}^{t-\Delta t/2} + \Delta t \ddot{x}^{t} \qquad \text{(Velocity)}$$

$$x^{t+\Delta t} = x^{t} + \Delta t \dot{x}^{t+\Delta t/2} \qquad \text{(Coordinates)}$$

Figure 2.3 Approximation of velocity and coordinates in central difference method.

1) Structural data and initial conditions: M, $x^0 = x(t=0)$ and $\dot{x}^{-\Delta t/2} = \dot{x}(t=0)$.

2) Compute internal force F_{int}^t

$$f_{e\ \text{int}}^{\ t} = \int_{V_e} B^T \sigma^t dV \qquad \text{(element internal force)}$$

$$F_{\text{int}}^{\ t} = \sum_e f_{e\ \text{int}}^{\ t} \qquad \text{(assemble into global)}$$

Here, for constitutive properties, the radial return method will be used in the incremental method to get σ^t.

3) Update external force and get acceleration

$$\ddot{x}^t = M^{-1}(F_{ext}^t - F_{\text{int}}^t)$$

4) Update velocity and displacement

$$\dot{x}^{t+\Delta t/2} = \dot{x}^{t-\Delta t/2} + \Delta t \ddot{x}^t$$

$$x^{t+\Delta t} = x^t + \Delta t \dot{x}^{t+\Delta t/2}$$

5) Repeat step 2 to 4 until analysis is done.

Table 2.4 Central difference algorithm.

I Initialization

(i) Determine Δt based on specified cycles, N, and simulation time t_f, $\Delta t = (t_f)/N$

(ii) Evaluate mass matrix M for each element based on stable time step

II At cycle t for load increment i.

(i) $\ddot{x}^t = M^{-1}(F^t_{ext} - F^t_{\text{int}})$

(ii) Evaluate components of damping factor C' based on either mass proportional or displacement form

$$C' = f(\omega^t, u^t)$$

$$\dot{x}^{t+\Delta t/2} = \frac{(1-0.5(C'_t)^t \Delta t)\dot{x}_t^{t-\Delta t/2}}{(1+0.5(C'_t)^t \Delta t)} + \frac{\Delta t \ddot{x}_t^t}{(1+0.5(C'_t)^t \Delta t)}$$

(iii) $x^{t+\Delta t} = x^t + \Delta t \dot{x}^{t+\Delta t/2}$

$$u^{t+\Delta t} = u^t + \Delta t \dot{x}^{t+\Delta t/2}$$

(iv) Update external force vector F^t_{ext}

(v) Obtain current internal force vector $F^{t+\Delta t}_{\text{int}}$ and current stable time step Δt_{cr}

(vi) Update mass if $\Delta t_{cr} < \Delta t$

(vii) Obtain current estimate of ω^t

$$K^t_{ii} \approx [F^{t+\Delta t}_{\text{int}\,i} - F^t_{\text{int}\,i}]/\Delta t \dot{x}_i^{t+\Delta t/2}$$

$$K^t_{ii} = \max(K^t_{ii}, 0)$$

$$\omega \equiv \left[\frac{\sum K^t_{ii}(u^t_i)^2}{\sum M_{ii}(u^t_i)^2}\right]^{1/2}$$

(viii) Go to II(i) and repeat

Table 2.5 Hybrid explicit solution algorithm (R. G. Sauve and D. R. Metzger, 1996)

CHAPTER 3

MATERIAL PROPERTIES DETERMINATION

The punch test combined with finite element analysis provides a technique for the determination of material properties. From a direct numerical analysis, a predicted load-deflection curve can be obtained with trial material properties. A difference will generally exist between the measured and predicted curve. The predicted response then can be fitted to the experimental response using a curve fitting algorithm, and the material properties can be determined.

Because of the nonlinear assumption, the stress-strain relation of the specimen cannot be determined from the experimental data directly. The strain energy, corresponding to the work of the punch load, can be used instead of the load-deflection. Based on the conservation of energy, during the punch test, the work done by the ball punch should be equal to the strain energy of the specimen. The strain energy, which includes the stress-strain information, can be obtained from the numerical analysis. The nonlinear material properties then can be determined from fitting the strain energy to the punch work.

3.1 Methodology of Material Properties Determination

To determine the stress-strain curve, the least-squares regression is used to fit the internal strain energy vs. displacement with the assumption that plastic strain distribution does not depend on the hardening curve. For the general stress-strain relation the strain energy is given as

$$U = \int_V \int_\varepsilon \sigma(\varepsilon, a_k) d\varepsilon dV \tag{3-1}$$

where $\sigma(\varepsilon, a_k)$ is a function of strain ε and curve fitting parameters a_k, index k is the number of the parameters.

For the finite element model, the strain energy then can be approximately expressed as

$$U^{fe} \approx \sum_{i=1}^{ne} V_i \int_\varepsilon \sigma(\varepsilon, a_k) d\varepsilon \tag{3-2}$$

where V_i is the volume of the element, index i is the number of the elements.

The sum of the squares of the residual errors over time period t between the punch energy, which was measured from the experiment, and finite element strain energy is given as

$$S_r = \int_0^t [U^m(t) - U^{fe}(t)]^2 dt \tag{3-3}$$

where U^m and U^{fe} are punch test and FE energy respectively. This can be approximately expressed as the sum of the squares of the residuals over the number of the recording points

$$S_r \approx \sum_{j=1}^{npt} [U^m(t_j) - U^{fe}(t_j)]^2 \tag{3-4}$$

For a best fitting curve, the sum of the squares of the residuals must be minimized. Setting the derivatives with respect to each of the curve fitting parameters are equal to zero will result in a minimum S_r. The equation can be expressed as

$$\frac{\partial S_r}{\partial a_k} = 0 \tag{3-5}$$

The curve fitting parameters a_k then can be determined from the differential equations (3-5) which ultimately provide a set of algebraic equations.

The standard deviation is used for the measure of the spread between the measured and predicted curve. It can be expressed as

$$S_y = \sqrt{\frac{S_r}{n-1}} \tag{3-6}$$

where n is the number of the measured points.

To implement the material properties determination, the Ludwik empirical expression is used as the constitutive stress-strain model for the strain energy equation. Appendix A.1 gives the derivation using Ludwik expression. The FORTRAN program (Chapter 4), which was developed to implement the algorithm of the material properties determination, is based on this empirical expression.

3.2 Punch Work

The punch work is needed as the experimental data for the least-squares fit to the strain energy curve predicted from the FE analysis. The punch work can be integrated from the experimental load-deflection curve. This can be expressed as

$$U^m = W = \int_\delta P d\delta \tag{3-7}$$

where U^m is the measured punch energy, P is the function of displacement δ.

The punch force P and displacement δ can be measured directly from the punch test. To numerically integrate these discrete data, the numerical method has to be applied, so that the punch work can be obtained from the experimental load-deflection data. One of the popular numerical methods is the trapezoidal rule which gives the estimated punch work as

$$W \cong \frac{h}{2}\left[P(x_0) + 2\sum_{i=1}^{n-1} P(x_i) + P(x_n)\right] \tag{3-8}$$

where x is the displacement and h is the displacement interval.

This can be explained as: for every small displacement interval, the work can be estimated by the area of the small segment. The areas of each small displacement segment can then be added to yield the work for the entire interval.

The punch force vs. displacement curve from the experimental test is shown in Fig. 3.1. The punch work, which is calculated from the experimental data over the range from zero to the ultimate point, is shown in Fig. 3.2. This was used as the experimental punch energy data file for the FORTRAN program.

3.3 Finite Element Strain Energy

The internal strain energy can be obtained from the finite element analysis. It can be expressed as

$$U^{fe} = U^{p} + U^{e} \tag{3-9}$$

where U^{p} and U^{e} are plastic and elastic parts of strain energy respectively.

The elastic part strain energy is given as

$$U^{e} = U_{0}^{e} + U_{hg}^{e} \tag{3-10}$$

where U_0^e and U_{hg}^e are one point Guass quadrature and hourglass control parts of the elastic energy respectively. The hourglass part of the energy is induced by the hourglass stiffness, since the unified deviatoric hourglass control [21] is used in this analysis.

The strain energy from the FE simulation is shown in Fig. 3.3. The scaled strain energy from Fig. 3.3 at the very beginning time steps is shown in Fig. 3.4. This can be explained as, when the clamping pressure applied at the beginning (0.01-0.1 second), transient induced oscillations, and oscillations were damped out after the pressure became steady.

3.4 Clamping Energy

During the punch test, both ends of the specimen were subjected to high vertical clamping pressure. This high clamping pressure, which is also simulated in the finite element analysis, is not part of the energy under the experimental load-deflection curve, therefore not part of the response to be fit. However, since the finite element model includes the clamping energy, it must be counted as part of the total internal energy of the specimen. This can be expressed as

$$U^{total} = U^{fe} + U^{clamp} \tag{3-11}$$

Based on the strain energy equation, the clamping energy in the finite element model can be calculated from

$$U^{clamp} = \sum_i V_i \int_0^{\varepsilon_i} \sigma(\varepsilon)\, d\varepsilon \tag{3-12}$$

where stress $\sigma(\varepsilon)$ is the function of strain ε, V_i is the volume of the element, index i is the number of the element. For linear elastic material, Hooke's law is applied, which gives

$$U^{clamp} = \sum_i V_i \left(\frac{1}{E} \int_0^{\sigma_1} \sigma\, d\sigma\right) = \sum_i V_i \left(\frac{\sigma^2}{2E}\right) \tag{3-13}$$

where E is the Young's modulus.

In this chapter, the methodology of the material properties determination is discussed. To determine the stress-strain curve of the unknown material, experimental punch energy data is fitted to the internal strain energy data from the finite element simulation using the least-squares method. The punch energy data is integrated from the punch test load-deflection curve using the trapezoidal rule. The Ludwik empirical expression is used as the constitutive stress-strain model for the strain energy equation. The implementation of the methodology will be discussed in next chapter.

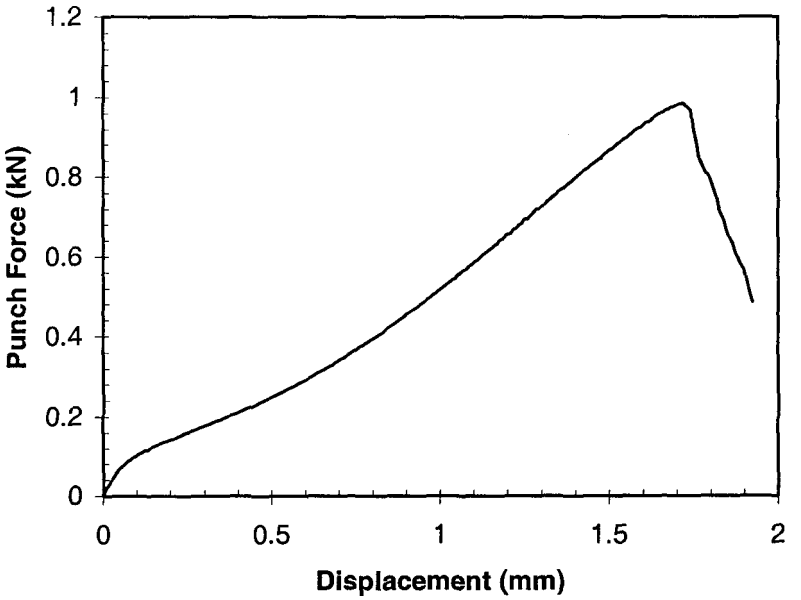

Figure 3.1 Experimental load-deflection curve.

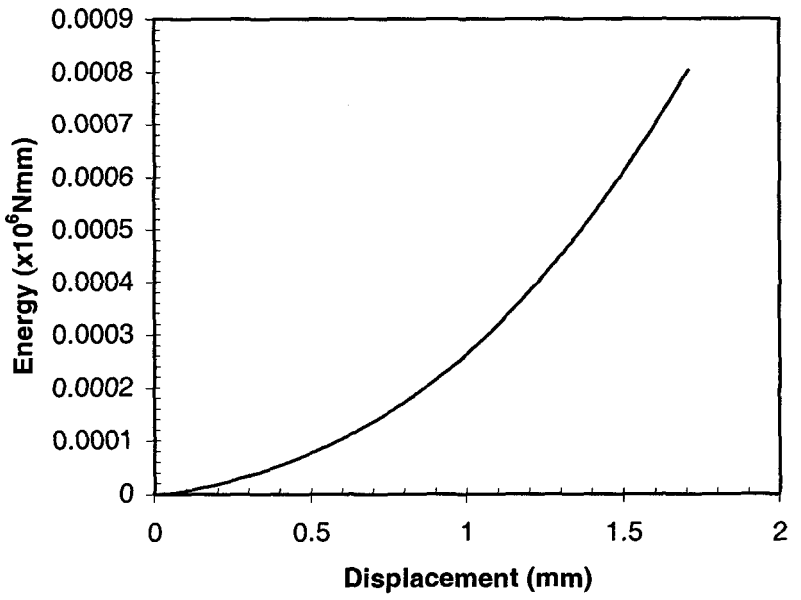

Figure 3.2 Calculated punch work from the experimental data.

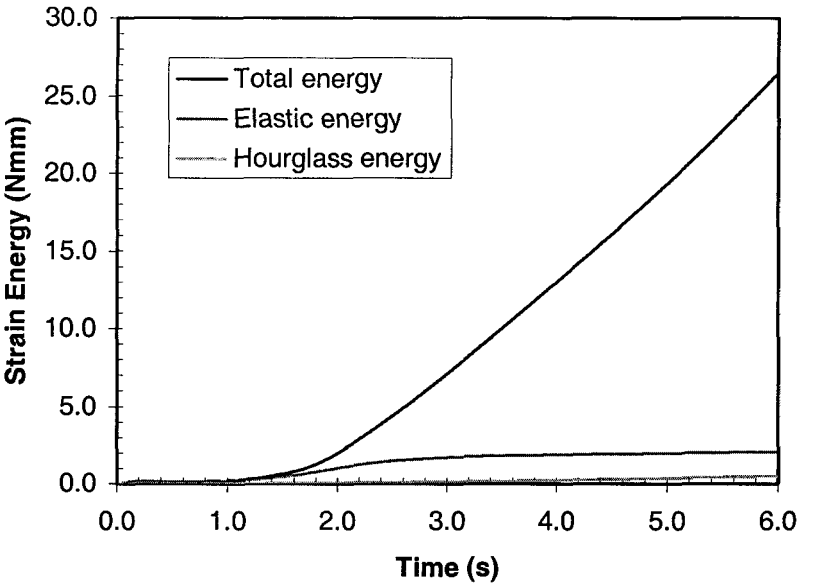

Figure 3.3 Strain energy from FE simulation.

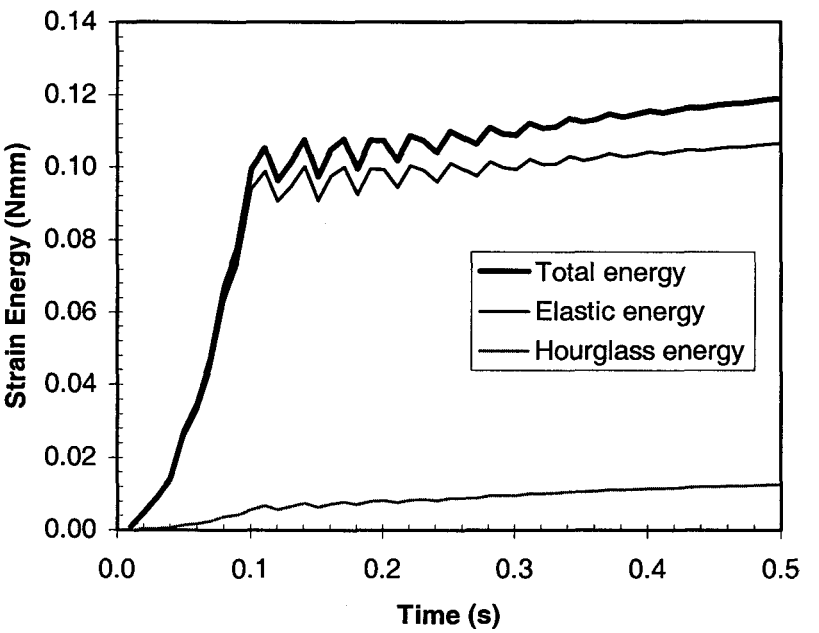

Figure 3.4 Strain energy at the very beginning time steps.

CHAPTER 4

SMALL PUNCH TEST

Small punch specimen techniques [23,24] have been used to determine material properties for a number of years. However, most of the tests were designed as a ball punch on a circular disk which was not applicable to anisotropic materials. A new designed test based on a small ball-punch-on-rectangular-specimen concept was used in this study. Since the specimen is not axisymmetric, a fully three-dimensional finite element model is required for the punch test simulation. To establish an effective finite element model, the punch test model needs to be validated by comparison with experimental results to prove its reliability.

4.1 Experimental Method

A small ball-punch-on-rectangular-specimen test is applied to test materials. This new designed test has the advantage of measuring properties which are highly dependent on the local microstructure and orientation of the cracking plane. To control the orientation of the cracking plane, which was not possible in the ball punch on a circular disk design, this design used a ball punch and a vertically supported rectangular

specimen. This provides a higher level of constraint in one direction and would force the cracking plane to be along the shorter side of the specimen [12].

The experimental punch test was designed and conducted by Ontario Hydro Technologies [12]. Figure 4.1 shows the punch test fixture developed for the present series of tests. The fixture was made of stainless steel, age-hardened at 900 °F (482 °C). A pair of clamps of the fixture supported a small rectangular specimen, which the maximum size is nominally 10 mm in length, 4 mm in width and 0.5 mm in thickness. There are two 0.6 mm radius fillets in the center of the lower clamp as the lower die to prevent the specimen from cracking on the early deformation stage. Each test specimen was manually polished to 600-grit finish and always placed the same way into the punch fixture. To mark its orientation, each test specimen has different chamfer sizes at its upper left and right corners.

Cap head screws were used to assemble the punch fixture and could be used to apply a clamping force. To ensure the specimen was evenly clamped, the screws were sequentially tightened while gauging the gap between the upper and lower clamps. The specimen was subjected to a central load applied by a closed-loop servo-hydraulic test system. The load was transmitted to the specimen via a 2.4 mm diameter ball punch. The test was run under displacement control. The displacement of the actuator and the load were continuously monitored. The feed back signal and a manual override were available to stop the test after the maximum load was reached.

Two sets of punch tests were previously performed to obtain the load-deflection data (at Ontario Hydro Technologies) on the So8 steel specimens at temperature 150 °C and 310 °C respectively. Specimens for the tests were cut from a straight steel feeder pipe. In the following lecture, So8st150 and So8st310 are used to distinguish two types of specimens, where the 'st' designation is for material taken from straight part of the pipe as opposed to an elbow part.

Two pairs of uniaxial tensile tests were also conducted for So8 steel at two different temperatures. The 'So8st150' specimen showed a mean yield stress of $\sigma_y = 264MPa$ while the 'So8st310' specimen showed a mean yield stress of $\sigma_y = 200MPa$. Both types of specimens showed significant work hardening and Young's modulus close to the nominal value. Furthermore, these uniaxial tensile data were used for the validation of the finite element analysis. Because the necking in the tensile test specimens prevented precise determination of the curve at high strain, the stress-strain curve was extrapolated to strains much larger than the tensile data provided.

4.2 Finite Element Modeling

The finite element computer code H3DMAP [46] was used with the FEMAP pre- and post-processor for mesh generation and results processing. The H3DMAP code provides a novel solution technique based on explicit formulations for transient problems. An important feature of the explicit formulation used here is the ability to apply

displacement controlled loading at a boundary where large plastic deformation is occurring. In this way, the punch force is calculated from the sliding contact forces for each increment in displacement, even past the point of global geometric instability [12].

A three dimensional finite element model was used since the specimen geometry is not axisymmetric for this punch test. However, according to the symmetry of the specimen in the length and width direction, a quarter model was used for simulation. Fig. 4.2 shows the FE mesh prior to the application of the test load. The model of the specimen consisted of 10647 nodes and 9120 elements.

In producing the FE model to follow the experiment as closely as possible, the specimen was assumed to be in contact with the ball punch, upper and lower clamps and lower die (with small radius). Four sets of contact surfaces were introduced: 1) ball punch and specimen. 2) upper clamp and specimen. 3) lower clamp and specimen. 4) lower die and specimen. A new contact algorithm [40], which applied a new penalty stiffness treatment for master-slave contact surfaces, is used in the FE simulation to avoid spurious nonuniformity in contact pressure distribution encountered by typical contact algorithms. This aspect of the simulation significantly improves the accuracy of the analysis.

The specimen was modeled using three-dimentional isoparametric solid element, and assumed to be elastic-plastic material with Young's modulus $E = 180GPa$ and Poisson's ratio $\nu = 0.3$. In this simulation, the 5 mm in length, 2 mm in width 0.47 mm in thickness (quarter model) specimen was modeled based on the dimension of experimental test specimen. The fixture (ball punch, clamps and die) was modeled as shell elements.

Furthermore the ball punch was modeled as a rigid sphere constrained to translate in the vertical direction at a prescribed velocity (Fig. 4.3). The clamps were defined as isotropic elastic material for contact stiffness with Young's modulus $E = 200GPa$, Poisson's ratio $v = 0.3$, and no yielding occurring. A high vertical pressure load (about half of the yield stress) was applied to the upper clamp as the clamping pressure to the specimen. The function of the pressure vs. time is shown in Fig. 4.4. The lower die was also modeled as rigid body by fixing all degree of freedom. A coefficient of friction at the fixture-specimen interfaces of $\mu = 0.5$ was assumed to prevent slipping.

4.3 Validation of the FE Model

FE analyses and experimental tests were performed for the specimens. The use of FE analysis can only be justified if the FE model and method used properly represent the physical situation. The FE model shown in Fig. 4.2 was used to determine the load-deflection curves for specimens. The predicted load-deflection curves for the specimen type of So8st150 and So8st310 are shown in Fig. 4.5 and 4.6 respectively along with measurements obtained from test samples. The uniaxial tensile data measured from the specimens were used for the FE analyses to predict the loading curve of the punch test.

The FE results were validated by comparison with the experimental test data. The comparison shows a good agreement between the predicted and measured curve, although the model tends to slightly over predict the force consistently. This could be

caused by modeling support conditions that are somewhat stiffer than actual test conditions [12].

The distribution of effective plastic strain, which is measured by thickness reduction, in the specimen So8st150 just prior to failure is shown in Fig. 4.7. The magnitude of strain is 0.668 and occurs at a position off the center plane. Similarly, in Fig. 4.8 for So8st310 specimen the magnitude of strain is 0.637 and occurs at a position off the center plane. These also give good agreement between the FE model and tests.

4.4 Analysis Procedures

The purpose of the finite element analysis is to predict the true stress-strain curve for the unknown material without prior knowledge of its tensile properties. An elastic perfectly plastic material model is assumed at the beginning as a trial model for the unknown material. With this trial model, the finite element analysis results in a difference between the measured punch work and predicted strain energy which can be integrated from the load-deflection curve (discussed in Chapter 3). Using the least-squares method, this difference can be used to correct the assumed true stress-strain curve to obtain an estimate of the actual hardening curve. Fig. 4.9 shows the differences of load-deflection curve between test and predicted data.

By repeating the analysis with the estimated stress-strain curve as the new trial model, an improved hardening curve will be obtained. Fig. 4.10 shows the first and

second estimated stress-strain curves from the iterative analysis procedure. It shows a significant improvement between the first iteration curve and the second iteration one (about 50% reduction of the discrepancy between the first iteration and the experimental curve). The general procedures of the analysis are given in the flow chart in Fig. 4.11.

4.5 Sensitivities to Experimental Parameters

It is desirable that the punch test should show a high sensitivity to the parameters being measured and a low sensitivity to influence effects. The parameters in the present work include: Young's modulus E, the yield stress σ_y, the ball diameter d, and the coefficient of friction between the ball and the specimen and between the specimen and the die, μ. Brookfield *et al.* [1] have studied the sensitivity of the punch force F to the foregoing parameters using Taguchi experimental design method with the FE analysis. The study showed the low sensitivity of the Young's modulus E and the coefficient of friction μ; the moderate sensitivity of the ball diameter d; the high sensitivity of the yield stress σ_y. This can be used to guide the parameters setting of the finite element simulation in the present work.

In addition to the FE analyses for sensitivity to experimental parameters, Brookfield *et al.* [1] also did a series of physical tests to confirm that the sensitivity to the clamping force. The tests show a low sensitivity of the clamping force in a relative large range.

This is highly desirable since the clamping pressure in the punch test is relatively difficult to control manually with the cap screw fixture.

4.6 Curve-fitting Implementation

The strain information computed from the finite element simulation is fitted to the measured data to provide an estimate of the stress-strain curve for the material. A post-processing FORTRAN program was developed to implement this step. The least-squares regression is used as the curve-fitting algorithm. The power law equations are used to represent the stress-strain relation in this program. Starting with the input, the program asks for 6 input items:

1) H3DMAP output *.h3dmap_contact file which includes the coefficient matrix for the least square differential equations (see Appendix) and internal energy;
2) H3DMAP output *.xy_1 file which includes the displacement vs. time data;
3) The experimental punch energy data file (*.energy);
4) The number of tests in experimental data file;
5) The clamping energy;
6) Displacement range to consider.

The key part of the program is the solution for the curve fitting parameters. Three subroutines were developed for this solution:

1) Read coefficient matrix and energy data

The least squares fit component matrix and internal elastic energy are read into array A and UEL respectively. As the output of H3DMAP, the matrix and energy are generated every time interval. The matrix gives the basic components for the determination of the curve fitting parameters from the least squares fit differential equations. The elastic energy U^e is obtained from the internal energy entry. The clamping energy U^{clamp} is also added to the total energy U^{total} at this step.

2) Align experimental data with finite element output intervals

The finite element outputs cannot fit to the experimental data directly, since the time intervals are smaller than the experiment. To allow for consistent use of the FE and experimental data, the FE output needs to be aligned with the experiment data. The experimental energy vs. displacement data is read into array UX and DX respectively. The units of the energy are converted to be consistent with the finite element output. The finite element displacement vs. time data is read into array D and T respectively, and aligned via linear interpolation with the experimental energy vs. displacement data based on the finite element time interval. The schematic of the alignment is shown in Fig. 4.12.

3) Solve linear equations

Punch energy U^m is computed at this step from the aligned experimental energy subtracting the internal elastic energy U^e. Because the exponent n is set up as constant

looped over from 0 to 1, the power law expression becomes linear equation. With different values of n, the material property parameters are computed:

i) The yield point of elastic perfectly plastic fit was computed from exponent $n = 0$;

ii) The yield point and plastic modulus of linear fit was computed from $n = 1$;

iii) The yield point and hardening rate of the power law expression then were computed with n looped over the range 0 to 1. The bilinear fit plastic modulus was also computed from with setting the fore obtaining linear yield point as its yield point.

The sum of the squares of the residuals between the experimental and computed energy is minimized to the least to find the real value of the curve fitting parameters. Standard deviation is computed for all of the cases. The flow chart of the program is shown in Fig. 4.13.

After compiling, the executable file named 'powerfit' was generated, and can be used as a post-processing function of H3DMAP. The example of the result from the 'powerfit' is shown in Fig. 4.14.

The experimental method and the finite element modeling of the small punch test were discussed in this chapter. Analysis procedures for predicting the true stress-strain curve for the unknown material were illustrated. The implementation of the post-

processing FORTRAN program was introduced at the end. The predicted results using this program will be discussed in next chapter.

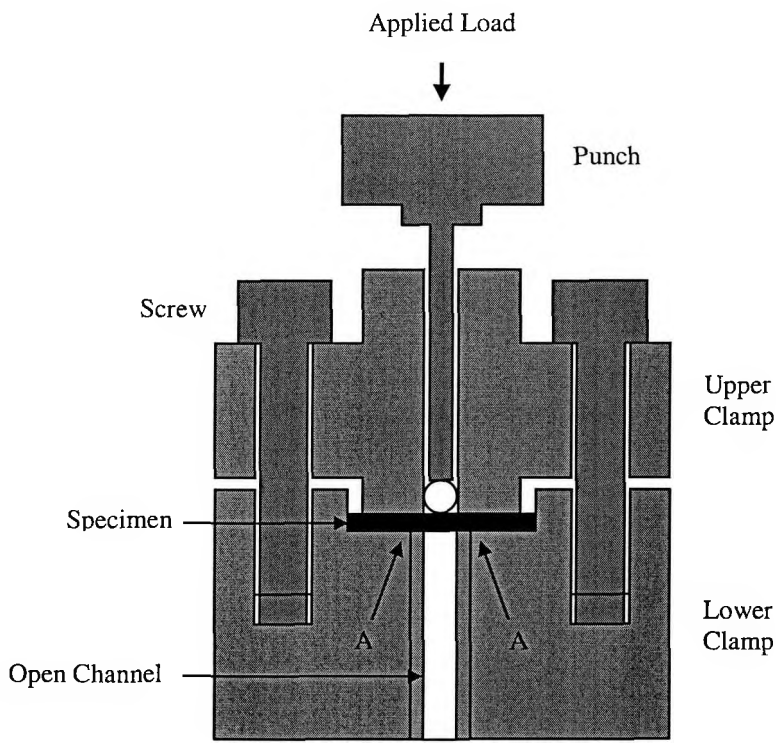

Figure 4.1 Schematic diagram of the punch fixture.

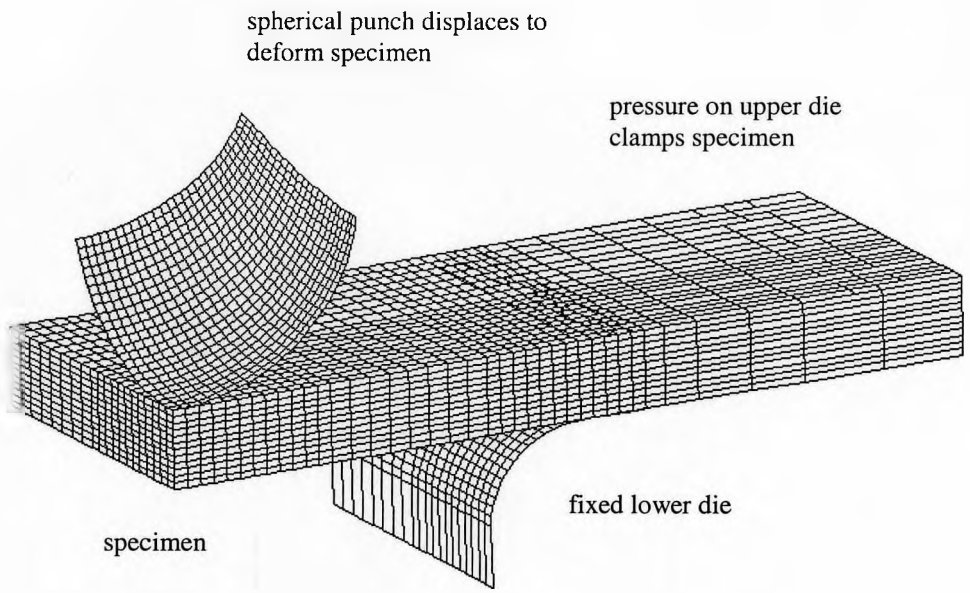

Figure 4.2 Finite element meshes for punch specimen and fixture (quarter model).

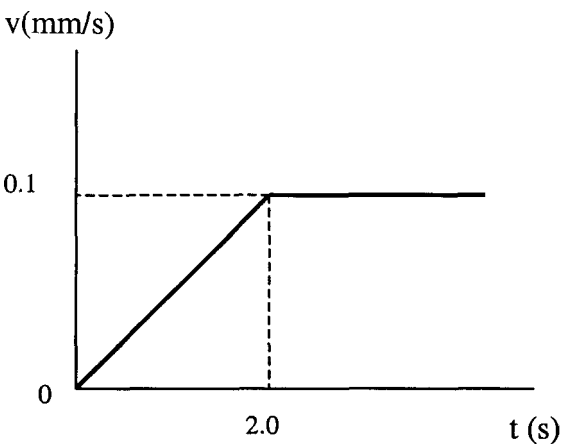

Figure 4.3 Ball punch velocity vs. time function.

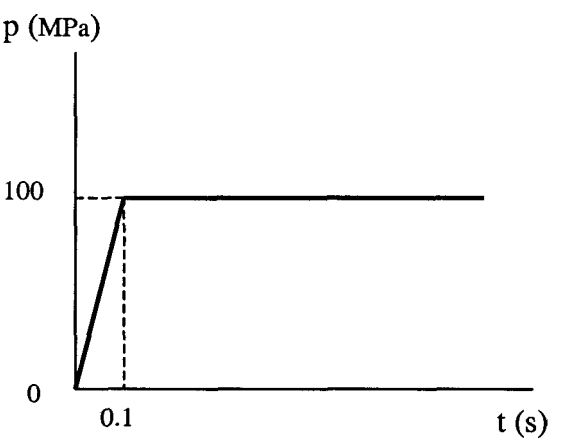

Figure 4.4 Pressure vs. time function.

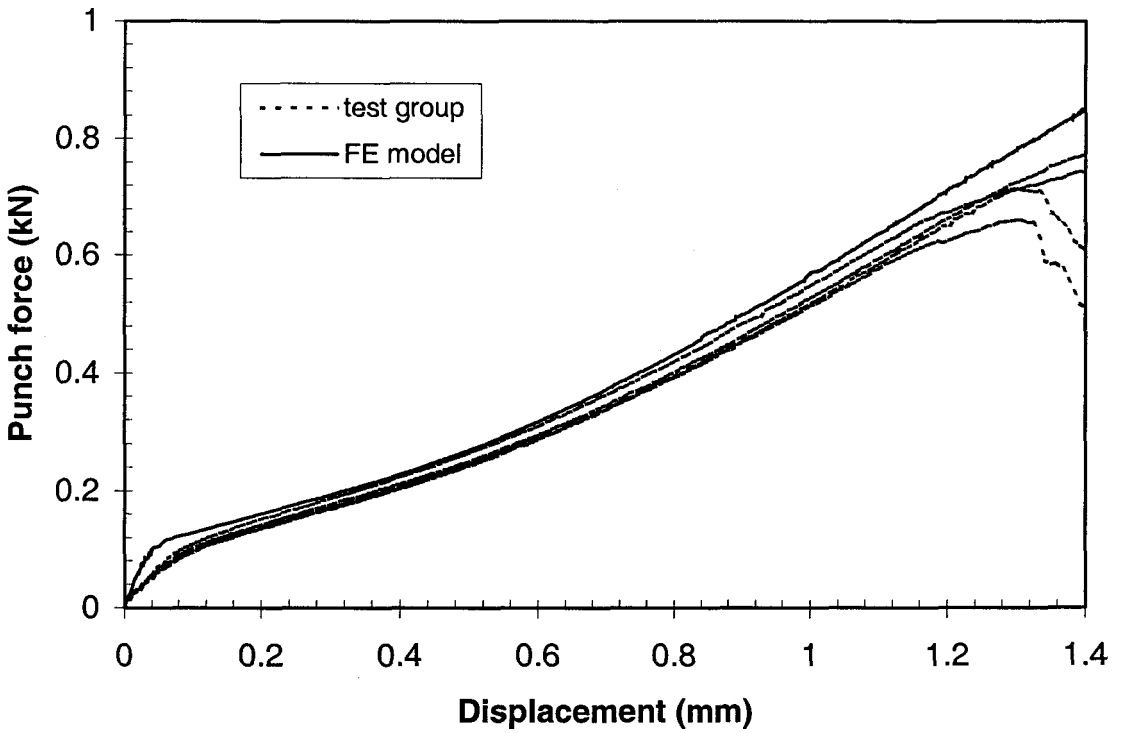

Figure 4.5 Predicted and measured load-deflection curve of specimen So8st150.

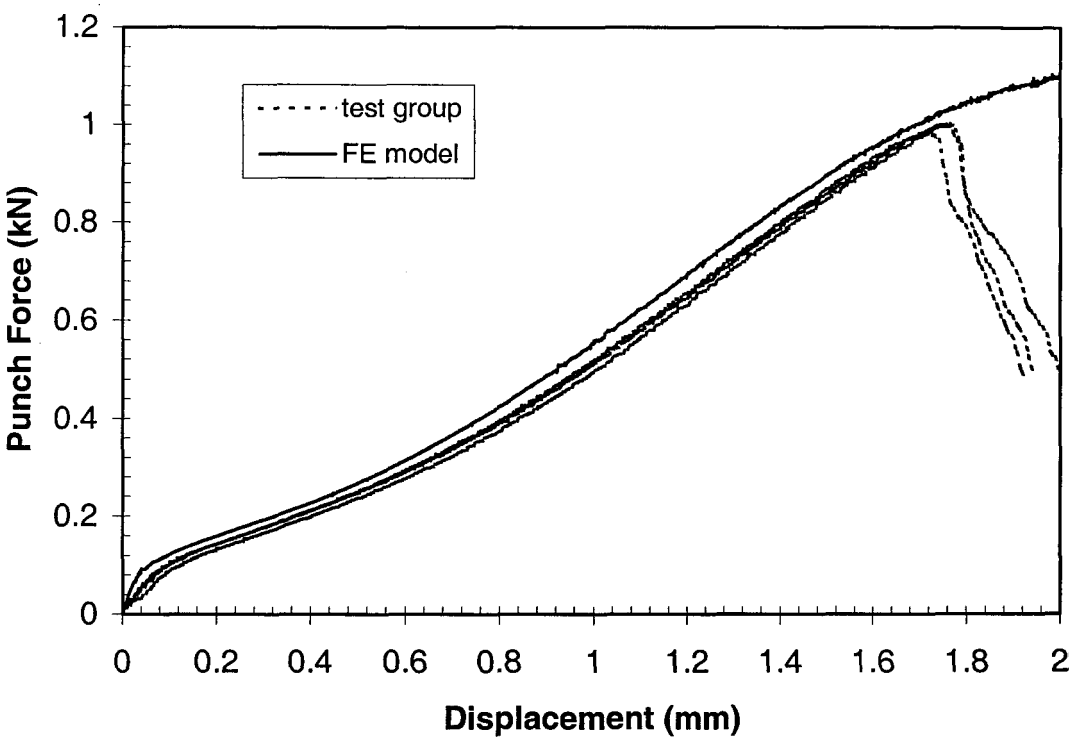

Figure 4.6 Predicted and measured load-deflection curve of specimen So8st310.

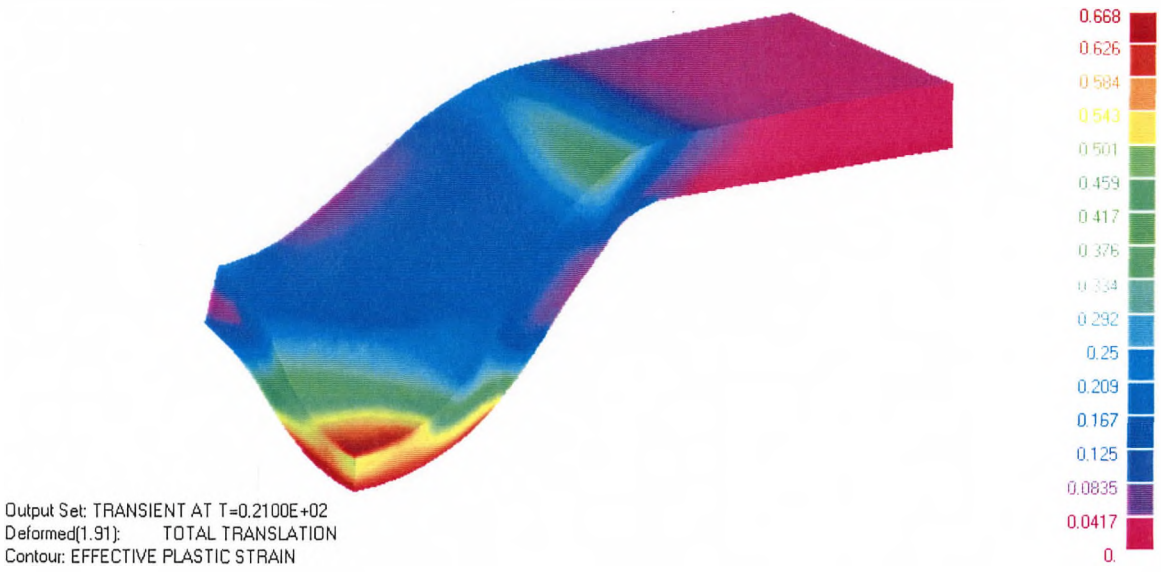

Figure 4.7 Effective plastic strain distribution in deformed specimen So8st150.

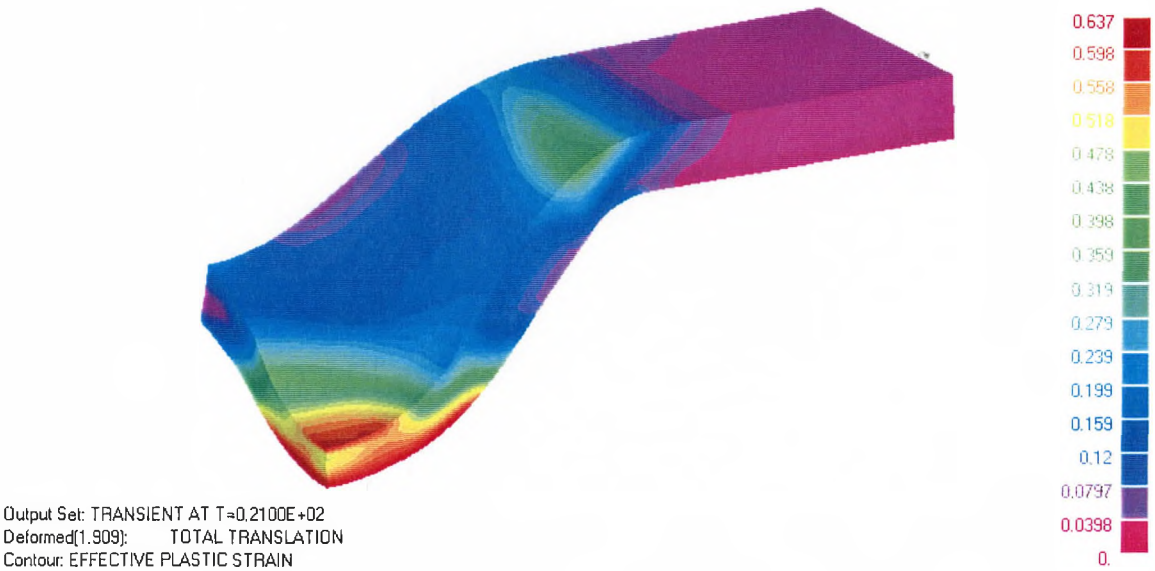

Figure 4.8 Effective plastic strain distribution in deformed specimen So8st310.

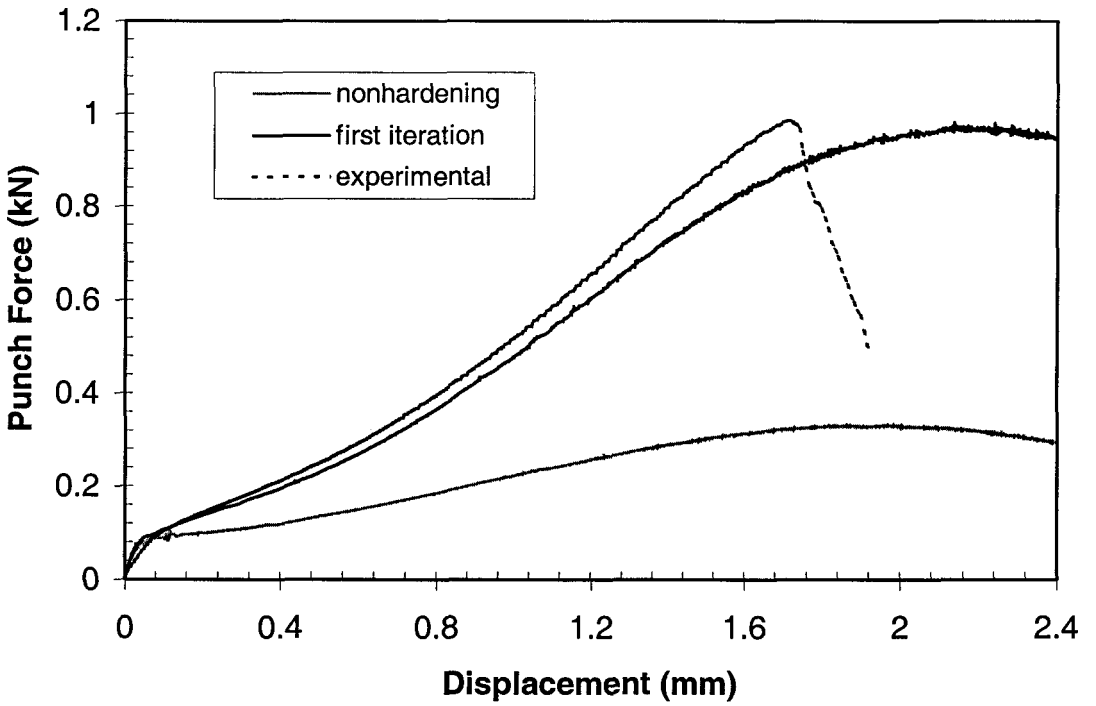

Figure 4.9 Predicted load-deflection curve from nonhardening trial model and first estimated stress-strain curve.

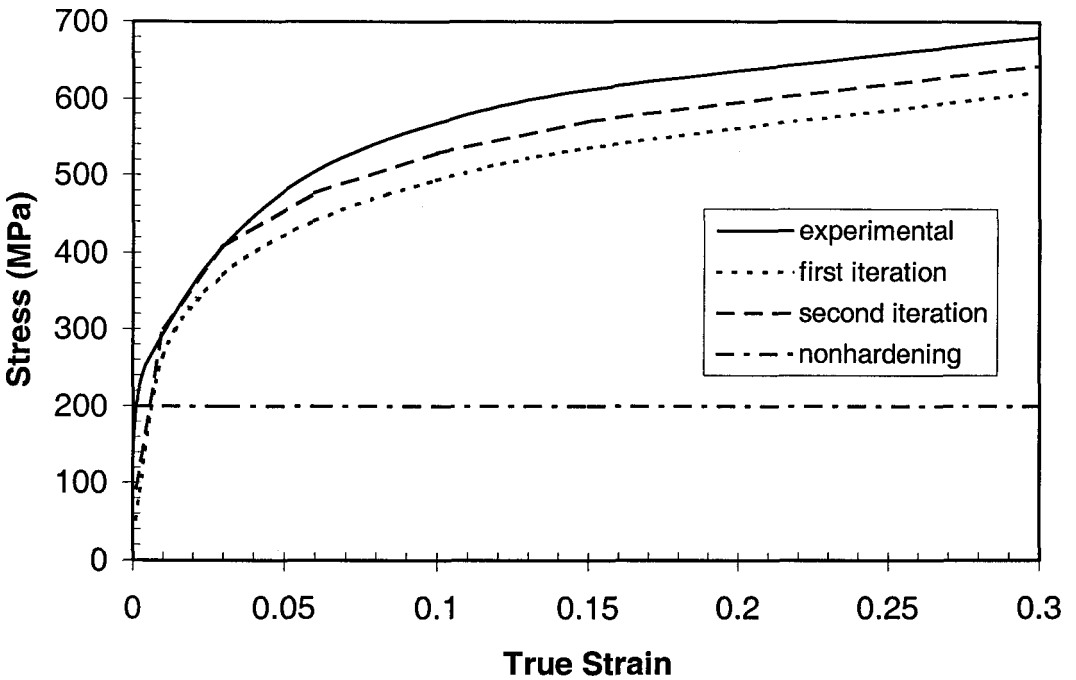

Figure 4.10 First and second estimated stress-strain curves from nonhardening trial model.

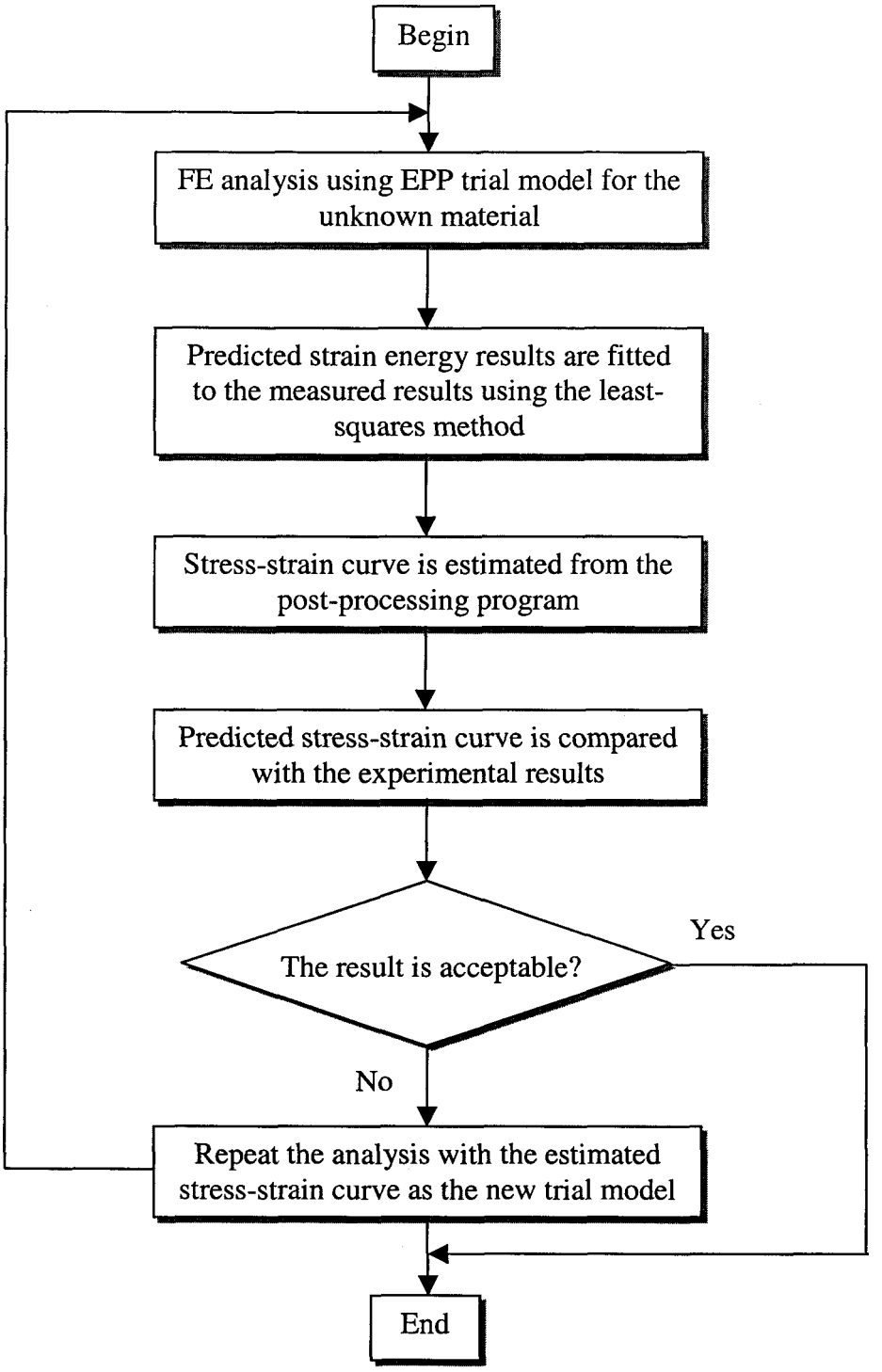

Figure 4.11 Flowchart of analysis procedures.

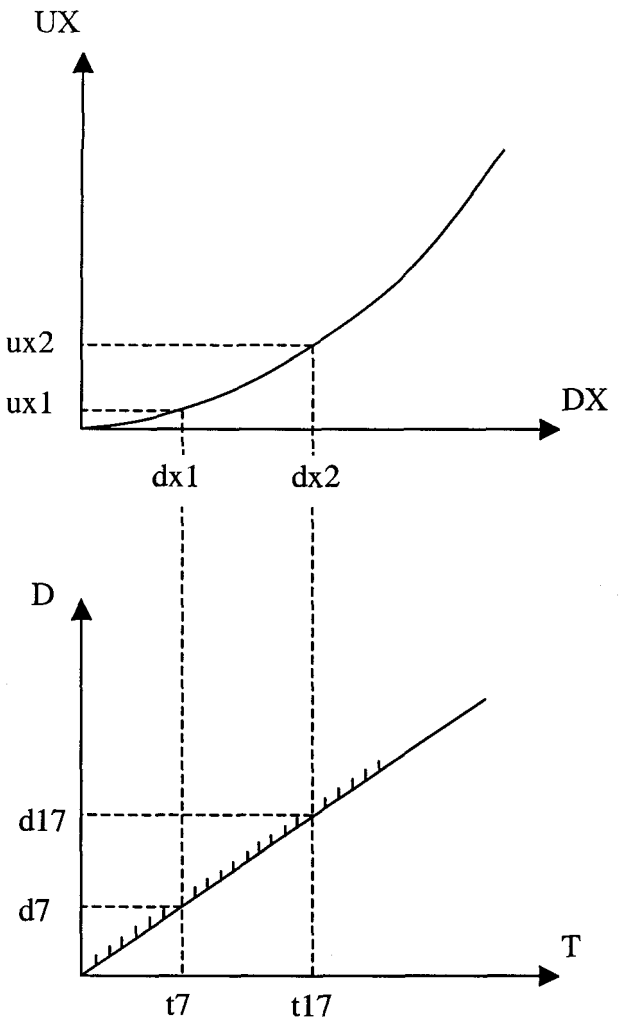

Figure 4.12 Schematic of predicted and experimental data alignment

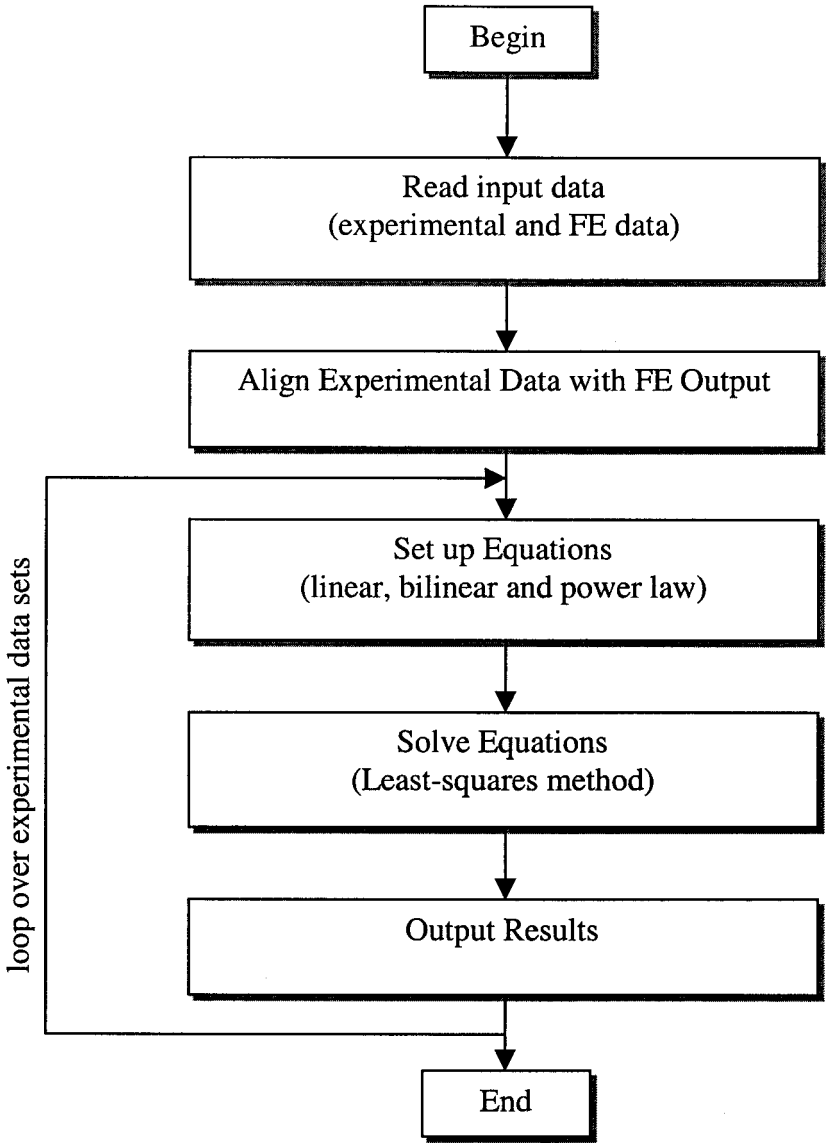

Figure 4.13 Flowchart of curve fitting program.

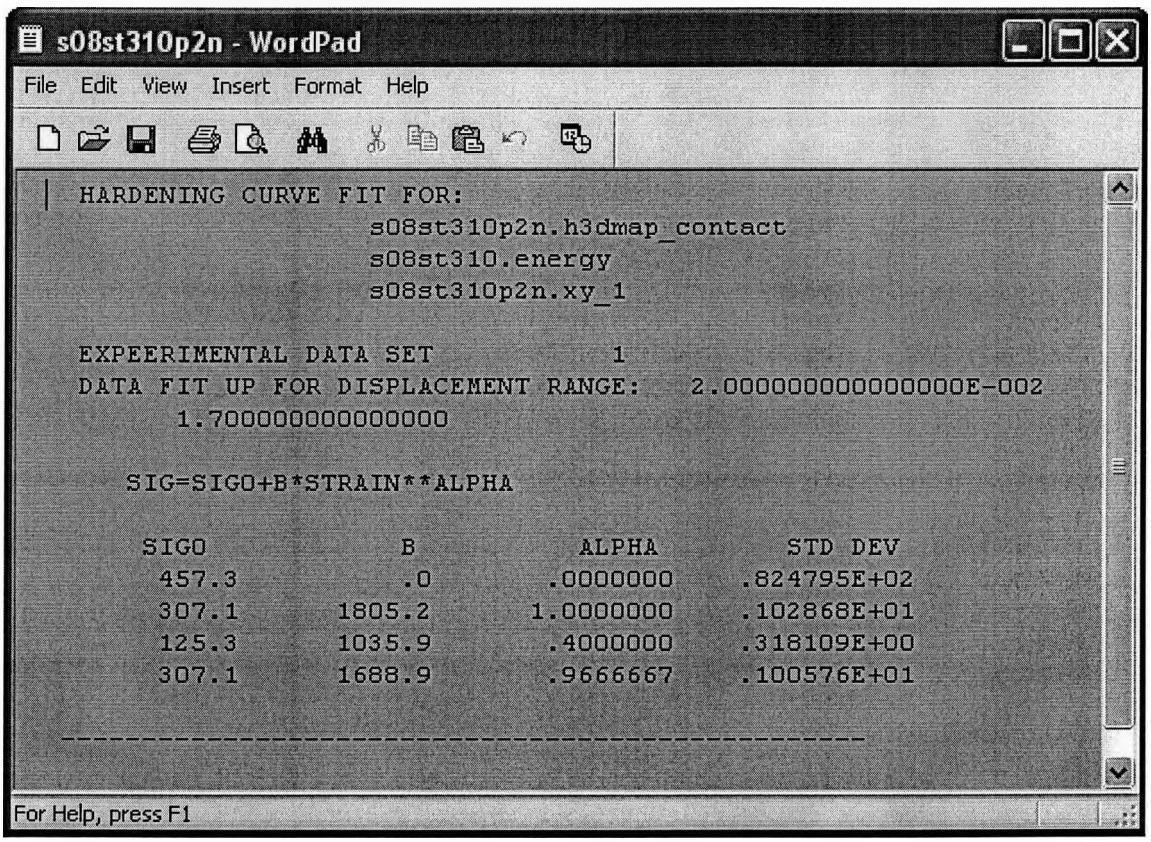

Figure 4.14 Result example from 'powerfit' post-processing.

CHAPTER 5

RESULTS AND DISCUSSION

The real value of the new small punch test is testing unknown materials. Without prior knowledge of the true stress-strain curve, the numerical simulation must proceed using assumed properties. To establish an effective set of parameters for the finite element analysis, two types of So8 steel specimens were tested by comparison with results from experiments. Once the parameters are obtained, the material properties can be determined from the finite element analysis combined with experimental results.

5.1 Elastic Perfectly Plastic Trial Models

Five trial models were tested for the prediction of the true stress-strain curve for specimen So8st150 and So8st310 respectively. All of the five models were assumed the elastic perfectly plastic material with the yield stress of 150, 200, 250, 300, and 400 *MPa* respectively. The power law fit curves computed from different trial models for specimen So8st150 and So8st310 are shown in Fig. 5.1 and 5.3 respectively.

The results show generally good agreement for yield stress up to 300 *MPa* models at the large strain field, although the curve for a yield stress 400 *MPa* is significantly above those at low yield stress. The yield points from bilinear fit of different trial models for two types of specimens are shown in Table 5.2 and 5.4 respectively. Both results show that higher predicted yield point will be obtained from the trial model with higher yield stress.

The experimental data of specimen So8st150 and specimen So8st310 showed a mean yield points of $\sigma_y = 264 \times 10^6 N/m^2$ and $\sigma_y = 200 \times 10^6 N/m^2$ respectively. Two elastic perfectly plastic models, which approximated to the mean yield point, with the yield points of 250 and 200 *MPa* respectively were chosen as the trial model for the following true stress-strain prediction.

5.2 Young's Modulus

Young's modulus has to be assumed for the punch test simulation. Since it is one of the influence effects and not the parameter being measured in this work, the Young's modulus is expected having a low sensitivity to the predicted results. Fig. 5.5 and 5.6 show the predicted stress-strain curves using different Young's modulus (160, 180 and 200 GPa) for specimen So8st150 and So8st310 respectively. Although there is roughly 10% difference between the Young's modulus, results show low sensitivity to the Young's modulus and are in agreement with Brookfield's [1] study.

5.3 Damping Coefficient

A hybrid explicit solution technique is used in this punch test simulation. Damping is required in order to remove undesirable inertia effects. Fig. 5.7 and 5.8 give the predicted load-deflection results for specimen So8st150 with damping coefficient 0.01 and 0.001 respectively. It is obvious that the punch force acting on the displacing part of the specimen reaches its highest value more smoothly with relative smaller damping coefficient. Throughout the analysis, a significant portion of the sample displaces at a roughly constant velocity. Inertial damping applied to this low frequency response results in high damping forces, which must be driven by high contact forces on the punch/specimen interface. For this reason, damping should be well below critical for the displacing part of the specimen [25].

5.4 Analysis Cycles

The punch test involves large impact and material deformation that are imposed by ball punch. The inertial effects in this case can be ignored (i.e. quasi-static), but the inertia forces need to be included in the transient formulation. In this analysis, the element density (hence mass) is scaled such that the critical time step for each element is equal to the final time (specified by the user) divided by the number of desired cycles. In this case, the inertial force related to the motion of the specimen is inversely proportional to the number of cycles (Table 5.9).

Fig. 5.10 shows the predicted true stress-stain curves with three different analysis cycles for specimen So8st310. The predicted curve had good improvement from 100,000 to 200,000 cycles, and little improvement from 200,000 to 300,000 cycles. The result shows larger number of analysis cycles offers more improvement in the predicted tensile curve, however this is not expected to offer much improvement with increasing numbers of analysis cycles. It must be noted that with larger numbers of analysis cycles the computation becomes more expensive, e.g. the running time of 200,000 cycles will be almost twice as long as that for 100,000 cycles.

5.5 Iteration Times

To predict the true stress-strain curve for the unknown material, the iterative finite element analyses were conducted. Without prior knowledge of the specimen's tensile properties, the elastic perfectly plastic trial model is used at the beginning for the finite element analysis. With the experimental load-deflection data (first iteration), the first predicted stress-strain curve could be obtained. Upon repeating the analysis with this first predicted stress-strain curve as the new trial model (second iteration), an improved true stress-strain curve could be obtained.

Fig. 5.11 and 5.12 show the iterative analyses results for specimen So8st150 and So8st310 respectively. The result shows that more iterations give more improvement of the predicted curve, but this is not expected to offer outstanding improvement with

increasing iteration times. Third iteration results from both figures show only a bit of improvement of the stress-strain curves. Furthermore, it is obvious that more iterations will make the computation become more expensive.

5.6 Power Law Fit

A power law fit (Ludwik expression), which is one of the most common methods of approximately representing the true stress-strain curve, was used to predict the tensile curve for unknown material. As discussed in chapter 1, this equation predicts a nonlinear work hardening stress-strain curve. Fig. 5.13 and 5.14 show the predicted true stress-strain and load-deflection curve for specimen So8st150 respectively. Similarly, Fig. 5.15and 5.16 show the results for specimen So8st310.

Following the direct analysis procedure, first estimated stress-strain curve computed from elastic perfectly plastic trial model with the nominal yield stress, $\sigma_y = 250MPa$ for So8st150 and $\sigma_y = 200MPa$ for So8st310, and 200,000 analysis cycles. For better results, the three times iterative analyses were conducted follow the same procedure using the new predicted stress-strain curve from last iteration as the trial model.

Comparison of predicted power law fit and load-deflection curve shows good agreement between the model and test, although the power law fit tends to underpredict at the early on strain stage. This could be caused by the mathematical form of the

empirical stress-strain equation since only three parameters are used for predicting the slope of the curve. Also, uncertainty in experimental load-deflection data at the beginning of the punch test represents higher relative error than for later response.

5.7 Bilinear Fit

The bilinear expression is also a common method of approximately representing the true stress-strain curve. With the linear expressions, the stress-strain curve can be easily obtained along with the yield point, and these could be used to correct the power law fit at the early on strain stage. Fig. 5.17 and 5.18 shows the comparison of bilinear fit and measurement for specimens So8st150 and So8st310 respectively. It gives reasonable predicted result at the early on strain stage (including the yield point) but yield stress gets too high at large strain with linear hardening. Combined with the bilinear fit at the early on strain stage, the modified power law fit results are shown in Fig. 5.19 and 5.20 for two specimen types respectively.

5.8 Ramberg-Osgood Fit

The Ramberg and Osgood fit is another frequently used method to approximate the true stress-strain curve. Fig. 5.21 shows the predicted true stress-strain curve for specimen So8st150 using Ramberg-Osgood fit. The bilinear fit was used to correct the

yield stress at the early on strain stage. Similarly, Fig. 5.22 shows the result for specimen So8st310.

Compared with the tensile test, the Ramberg-Osgood fit gives reasonable predicted yield point and stress at the early on strain stage (less than 12% for specimen So8st150 and 16% for So8st310), but much overpredicted stress later on. This could be caused by the mathematical model of the Ramberg-Osgood empirical equation, which is actually a special form of Ludwik fit. Appendix A.2 gives the algorithm of the Ramgerg-Osgood fit. With only two coefficients left, the predicted curve is forced to pass through the origin, and loss the accuracy occurs at large strain region.

5.9 Predicted Curves from Tensile Test

The true stress-strain curves derived directly from the tensile test data had been used to validate the finite element model before. For better results, 200,000 analysis cycles and two iterations of the analysis were used in the prediction. The power law fit was used to predict the true stress-strain curve. The results for the specimens at 150 °C (So8st150) and 310 °C (So8st310) are shown in Fig. 5.23 and 5.24 respectively. The measured stress-strain curves were extrapolated to strains much larger than the tensile data provided. Comparison of predicted power law fit and measurement shows very good agreement between the model and test.

In this chapter, two types of specimens were tested following the analysis procedures and compared with the experimental results. At the beginning, some key parameters for the finite element simulation were tested and successfully set up. Then the true stress-strain curves of the test specimens were obtained from the FE analysis and the post-processing curve-fitting program. Power law fit combined with the bilinear fit showed good agreement between the model and test in this study. At the end of this chapter, the true stress-strain curve were predicted directly from the tensile test data following the analysis procedures, comparison of the predicted and test results showed very good agreement, this is also validate the FE model and analysis procedures in this study.

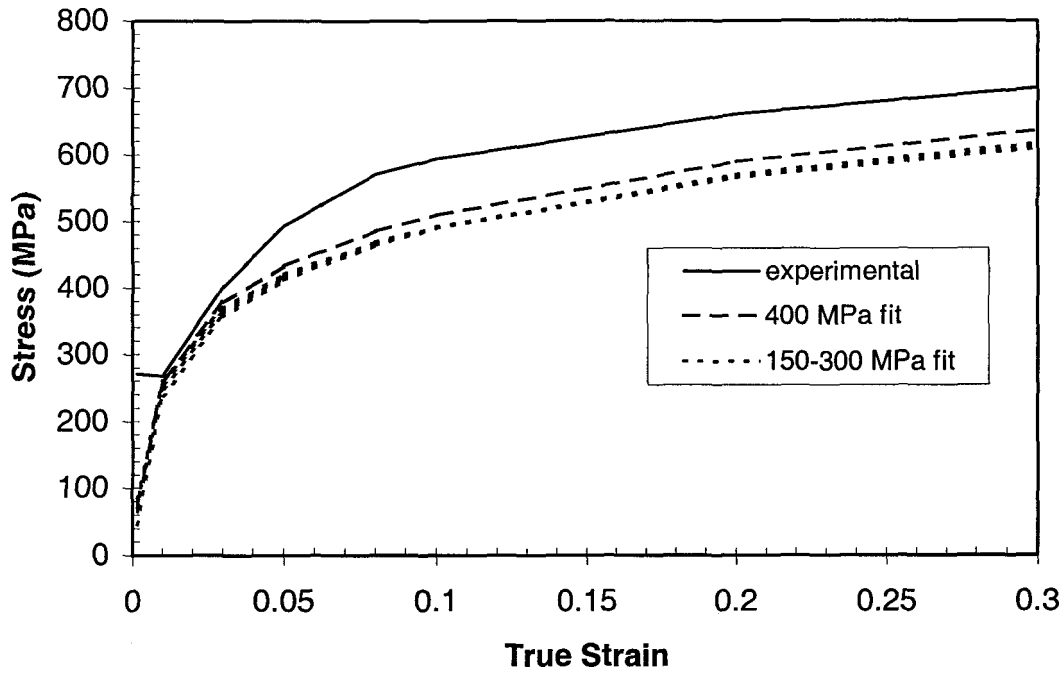

Figure 5.1 First estimated power law fit from different trial model for So8st150.

Unit MPa

Trial Model	150	200	250	300	400
Yield Stress	204.9	225	235	241.7	242.7

Table 5.2 Bilinear fit yield stress from different nonhardening trial model for So8st150.

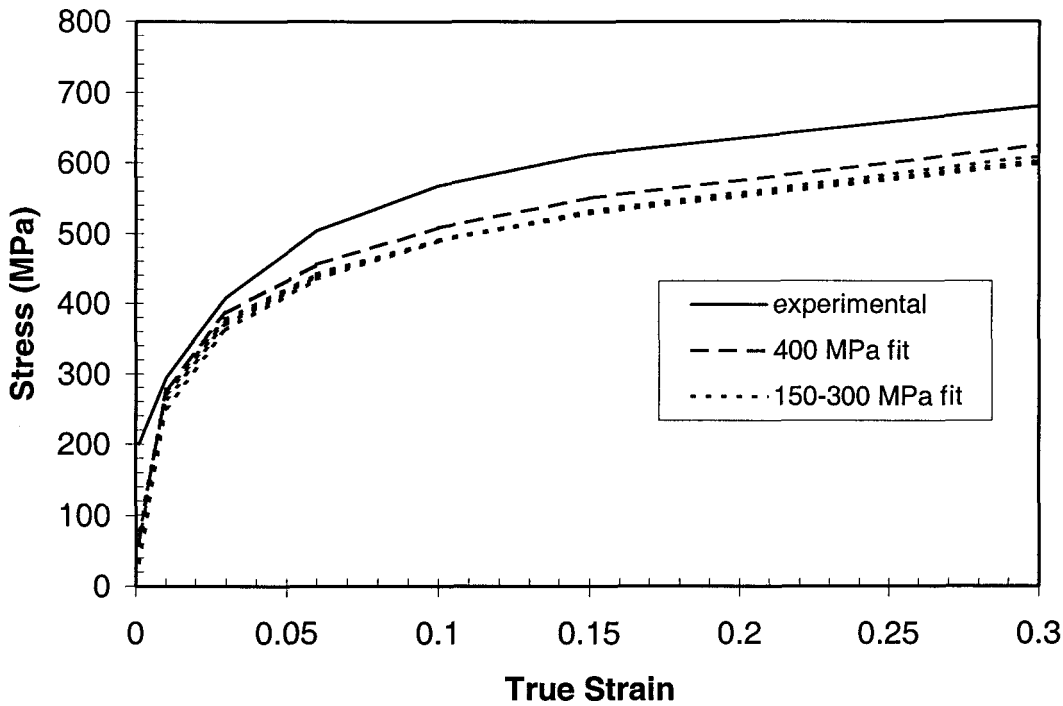

Figure 5.3 First estimated power law fit from different trial model for So8st310.

Unit MPa

Trial Model	150	200	250	300	400
Yield Stress	212.8	234.6	245.4	252.4	253.7

Table 5.4 Bilinear fit yield stress from different nonhardening trial model for So8st310.

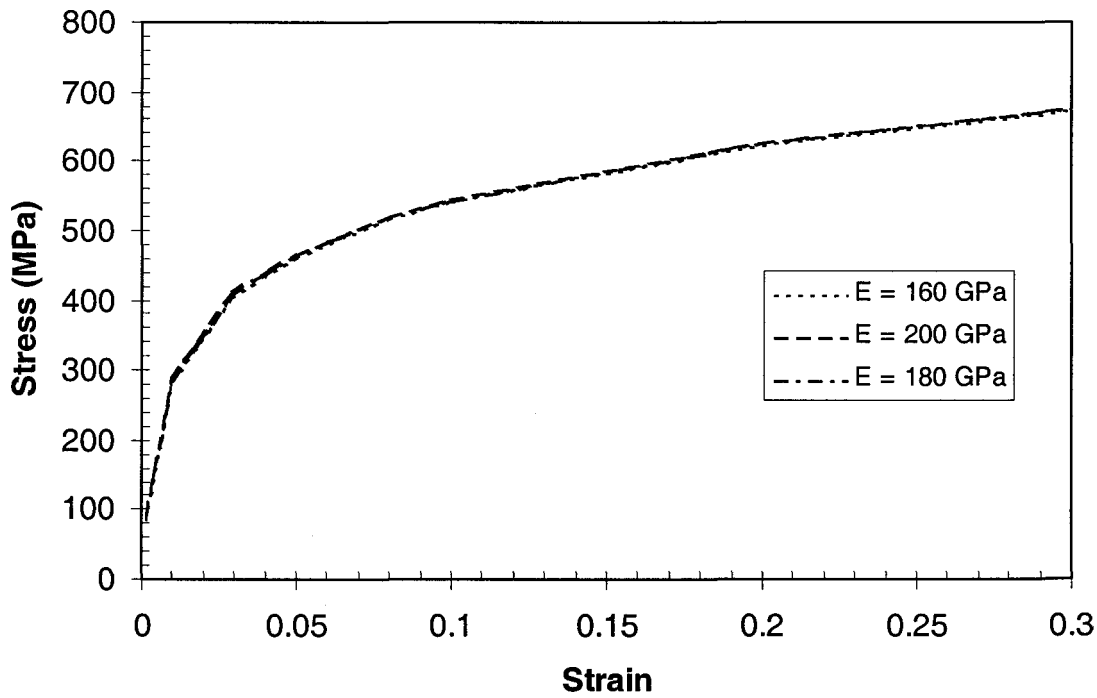

Figure 5.5 Stress-strain curve predicted from different Young's modulus for So8st150.

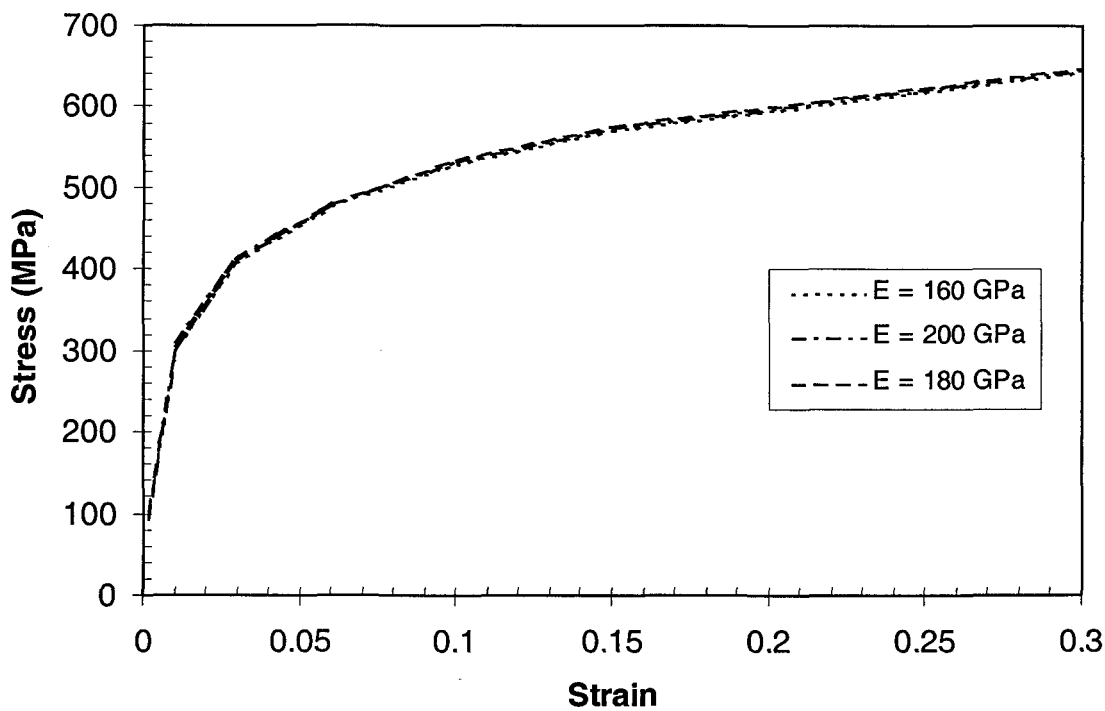

Figure 5.6 Stress-strain curve predicted from different Young's modulus for So8st310.

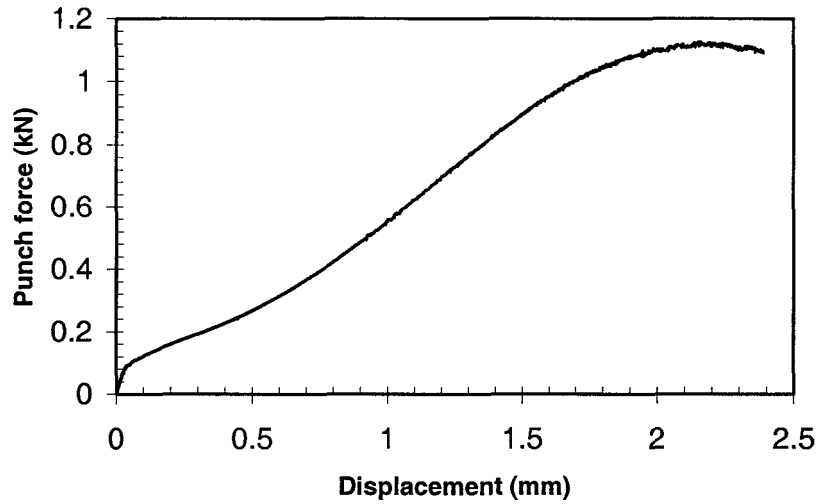

Figure 5.7 Load-deflection curve with damping coefficient = 0.001

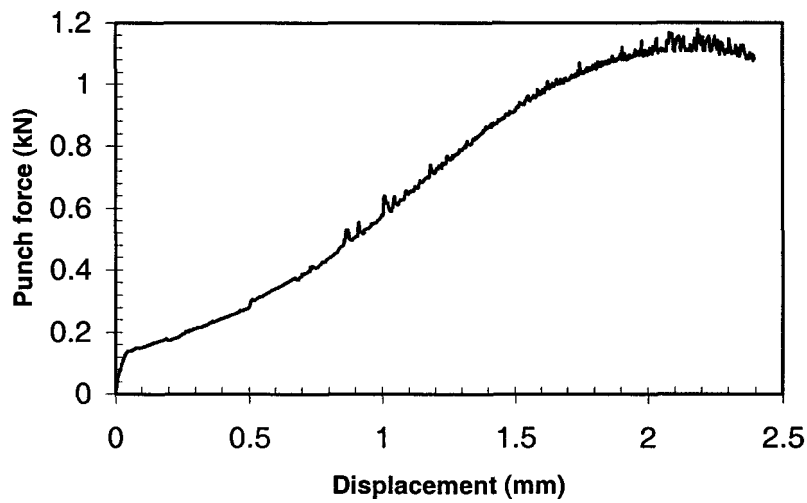

Figure 5.8 Load-deflection curve with damping coefficient = 0.01

Number of cycles	100,000	200,000	300,000
Time step	0.000113	0.0000575	0.0000373
Kinetic energy	0.029	0.0082	0.0033

Table 5.9 Time step and kinetic energy (motion) of different analysis cycles.

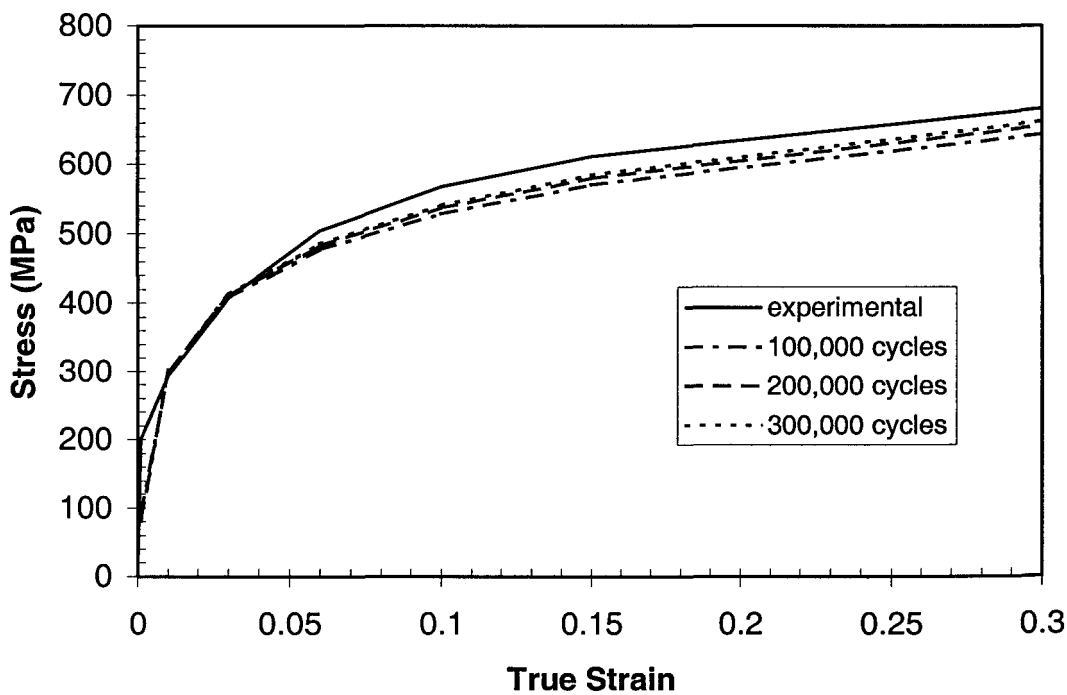

Figure 5.10 Comparison of true stress-strain curve from different analysis cycles.

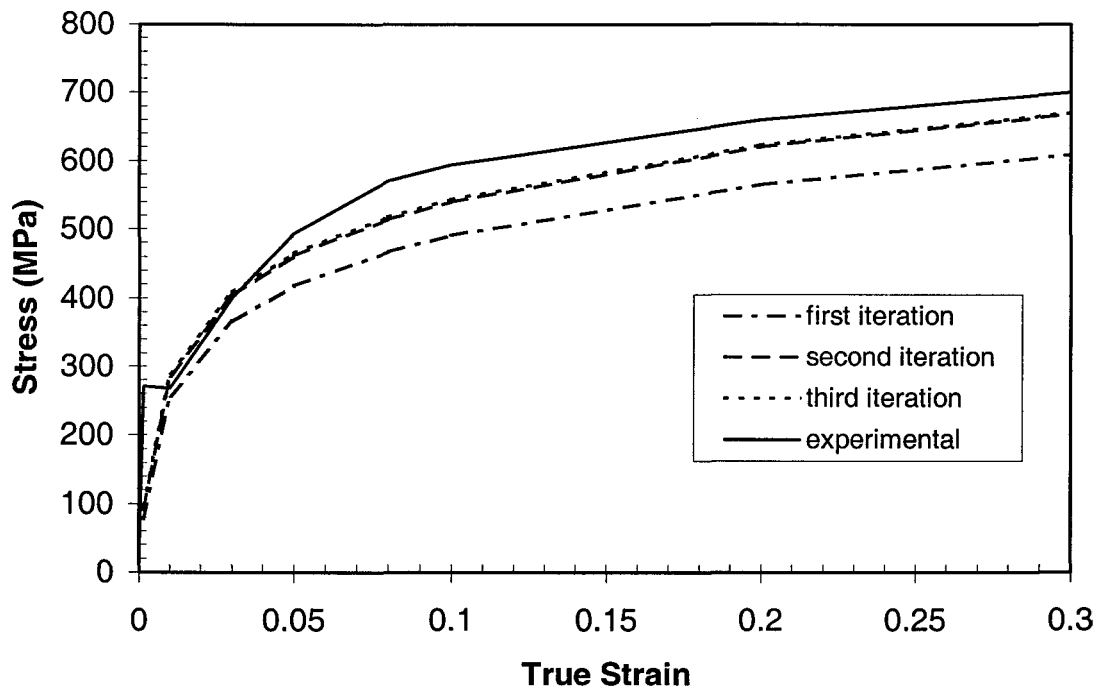

Figure 5.11 Comparison of different times iterative analysis for specimen So8st150.

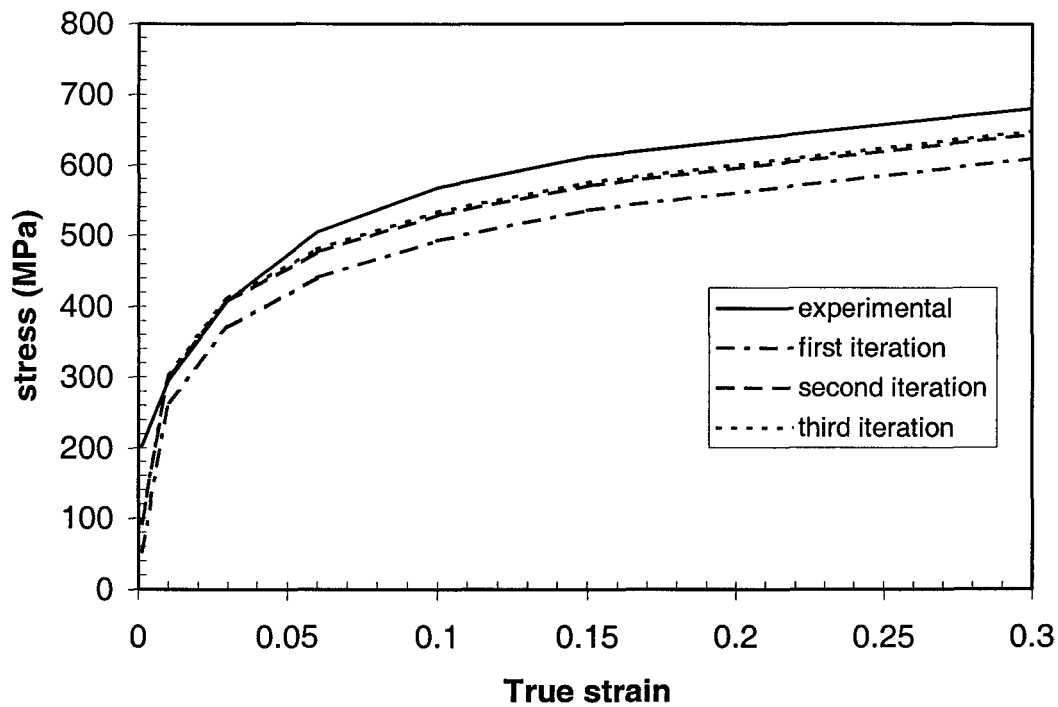

Figure 5.12 Comparison of different times iterative analysis for specimen So8st310.

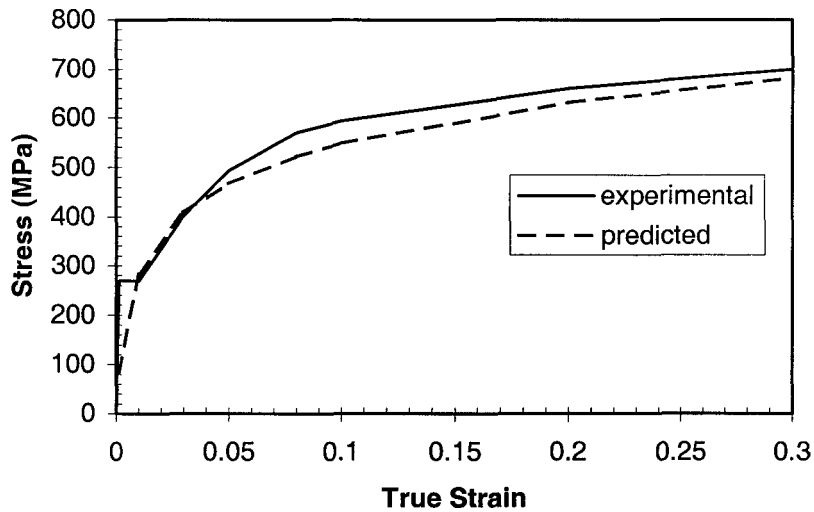

Figure 5.13 Power law fit for specimen So8st150.

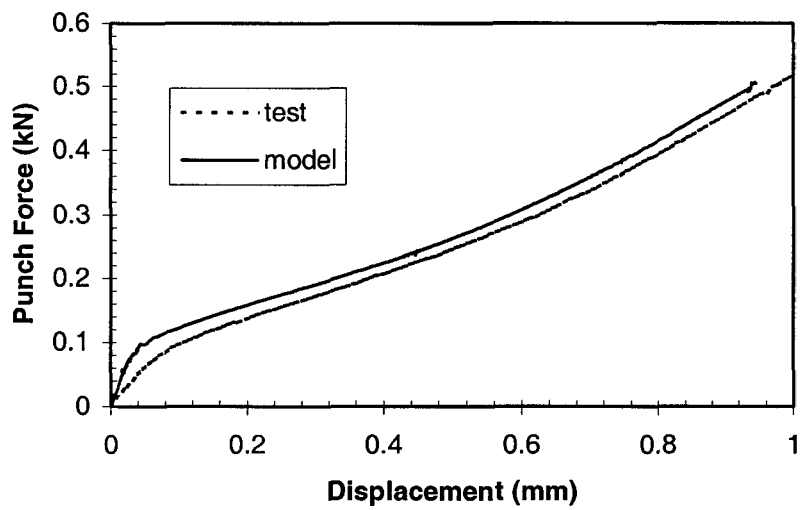

Figure 5.14 Comparison of measured and predicted load-deflection curve for So8st150.

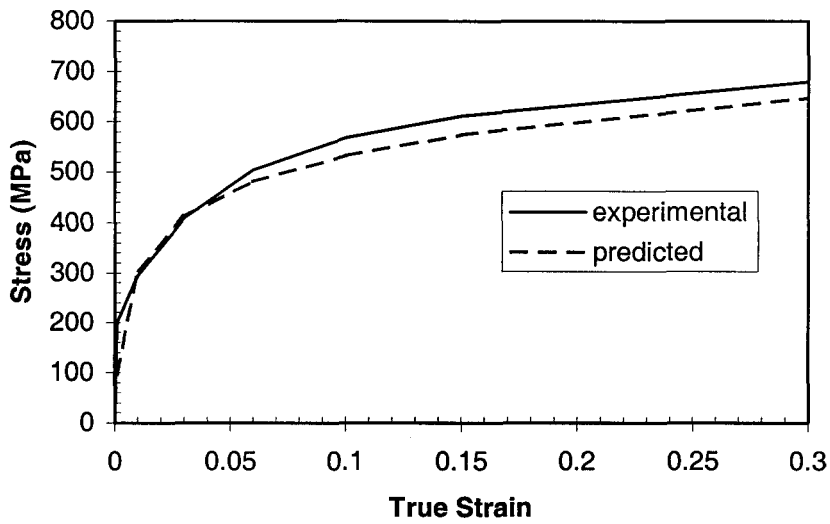

Figure 5.15 Power law fit for specimen So8st310.

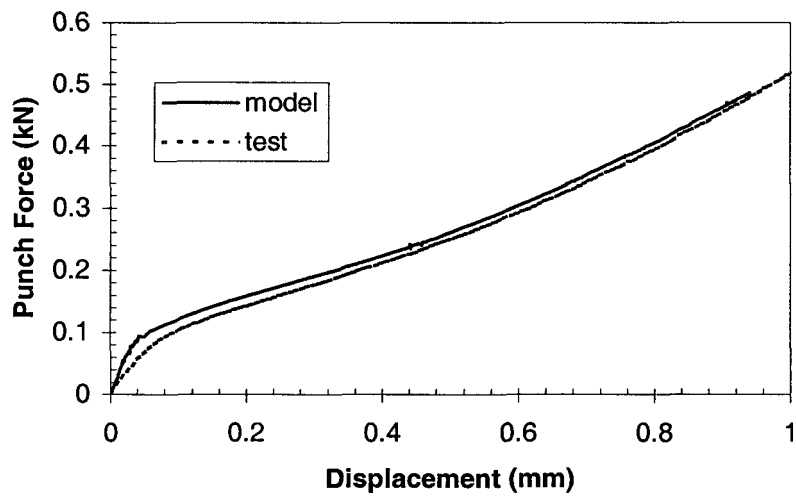

Figure 5.16 Comparison of measured and predicted load-deflection curve for So8st310.

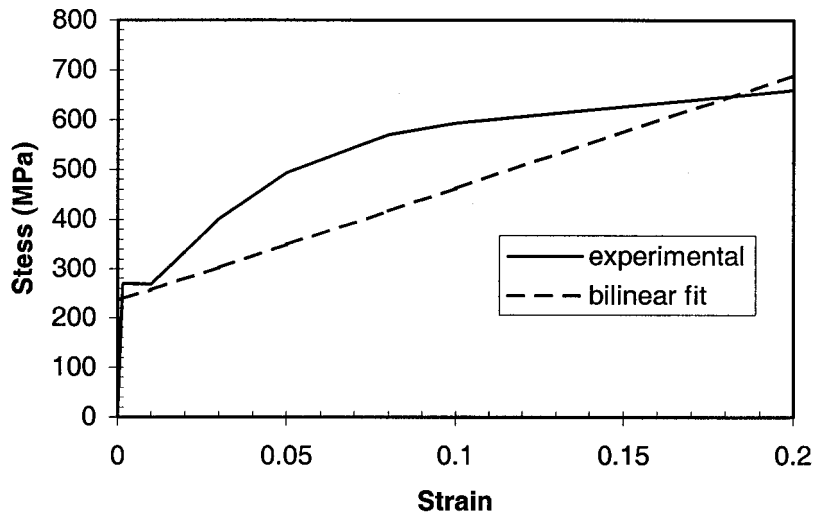

Figure 5.17 Bilinear fit for specimen So8st150.

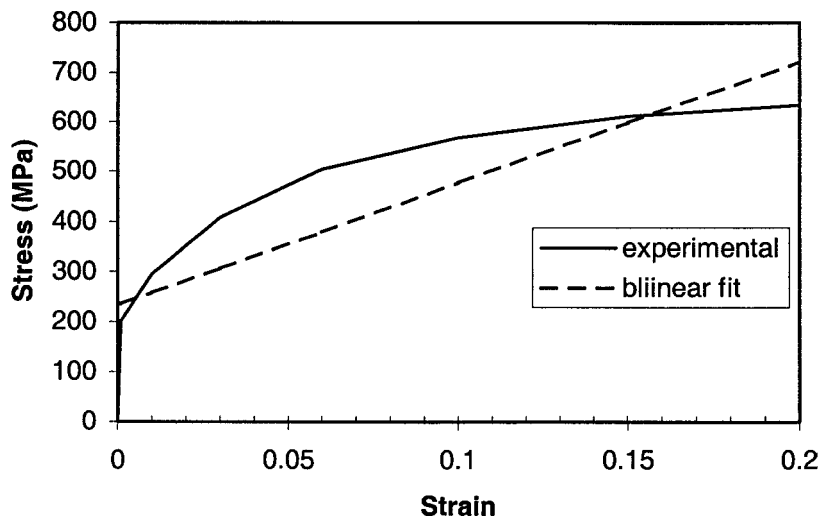

Figure 5.18 Bilinear fit for specimen So8st310.

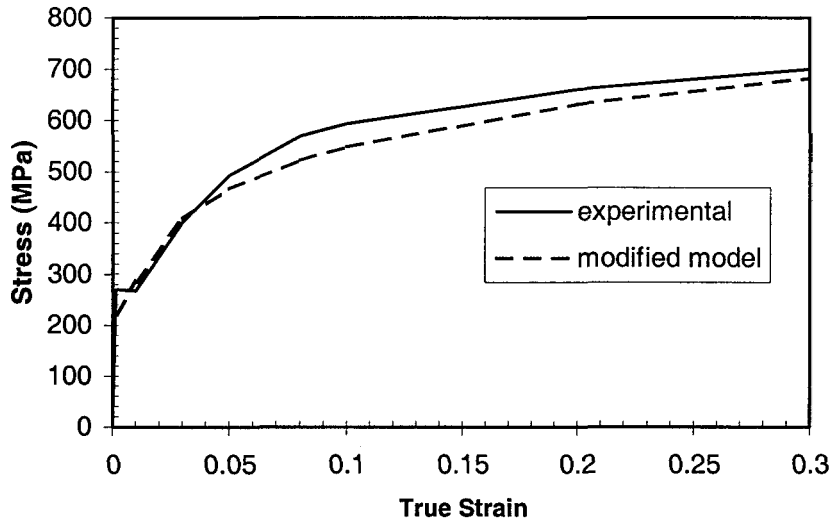

Figure 5.19 True stress-strain curve from modified trial model for So8st150.

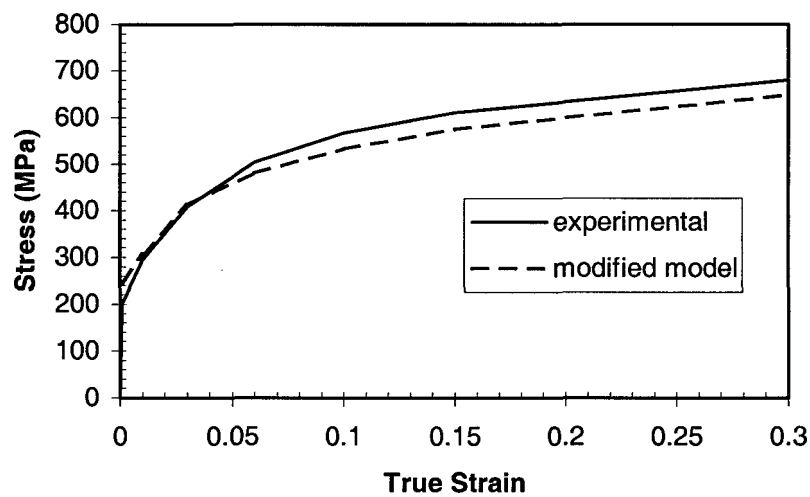

Figure 5.20 True stress-strain curve from modified trial model for So8st310.

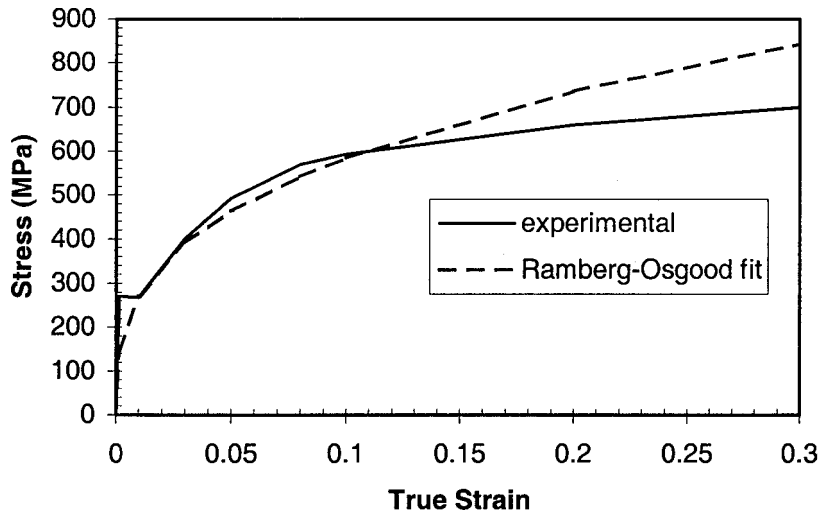

Figure 5.21 Predicted true stress-strain curve using Ramberg-Osgood fit for specimen So8st150.

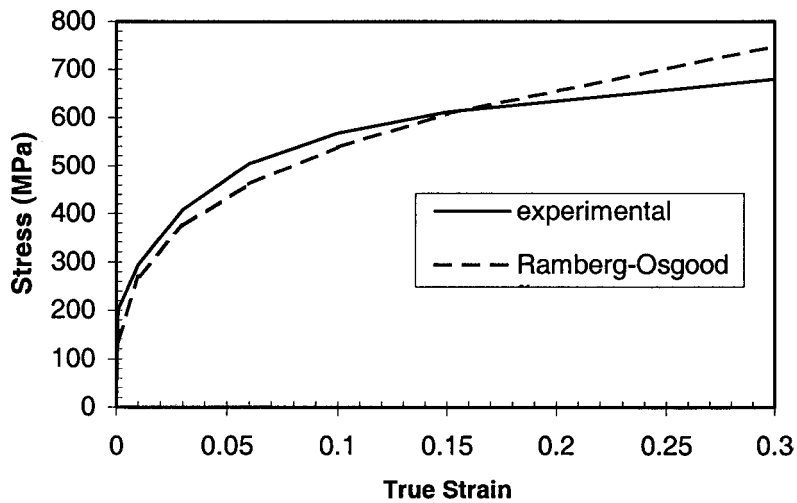

Figure 5.22 Predicted true stress-strain curve using Ramberg-Osgood fit for specimen So8st310.

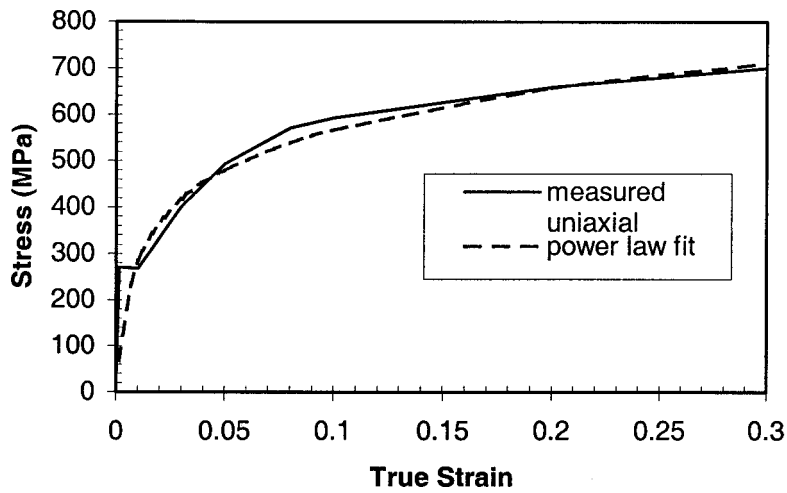

Figure 5.23 True stress-strain curve computed from tensile data for So8st150.

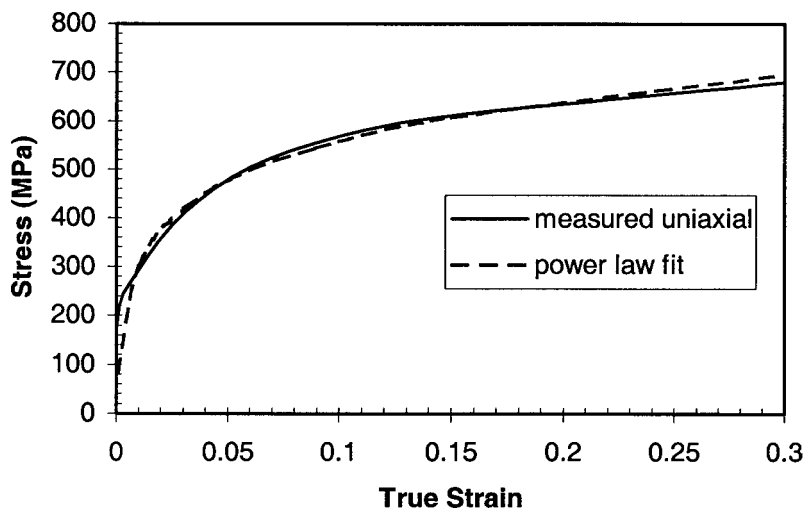

Figure 5.24 True stress-strain curve computed form tensile data for So8st310.

CHAPTER 6

CONCLUSION AND RECOMMENDATIONS

6.1 Conclusion

A new designed punch test for obtaining material properties from small specimens has been studied through finite element analysis and experiment. Using a ball punch and rectangular specimen, the punch test is applicable to anisotropic material. A three dimensional finite element model of the small punch test is required, since the specimen geometry is not axisymmetric. Analytic parameters, which are important to a validated finite element analysis, have been successfully investigated and applied to this analysis following the experimental procedures as closely as possible. The hybrid explicit procedure demonstrated the efficiency to the finite element simulation in the solution of complex three-dimensional nonlinear problems.

Two types of specimens cut from straight So8 steel pipe were examined as the unknown material. Using the empirical equations, the true stress-strain curves can be predicted by fitting the numerical results to experimental data. Power law fit (Ludwik expression) shows good agreement between the model and test. However, due to the

limitation of the mathematical model, there is an underprediction at the early on strain stage (around yield point and Luder's band). The power law fit combined with the bilinear fit has been used to improve the underprediction. Ramberg-Osgood fit gives reasonable predicted yield point and stress at the early on strain stage, but the stresses were overpredicted as strain increasing. This finite element model was very accurate in the prediction of the true stress-strain (less than 5% discrepancy after the Luder's band) and the load-deflection curve from given tensile test data using the power law fit.

6.2 Recommendations

The specialized program presents the capability to process punch test data with the general purpose finite element code. This program can be used to explore the possibility of using a fixed database for material characterization. Such an approach would need a database of strain, which is a function of position and time, for a range of material stress-strain curves so that any given material can be approximated through an interpolation process. This would provide a very fast way for a user to determine the stress-strain curve, as only a minimal number of inputs would be required in addition to the load-deflection data acquired from the punch test.

6.3 Future Work

The studies show the limitation of the true stress-strain curve prediction using the power law empirical equations since only three parameters are involved. Further elastic-plastic material models with more parameters can be considered for the estimating of the stress-strain curves. Since the new designed punch test has the capability to control the deformation along a desired orientation, anisotropic material properties can be studied by the punch test using strip specimens cutting in different orientation (circumferential, axial and thickness if possible). This also can be considered in the future.

REFERENCES

[1] D. J. Brookfield, W. Li, B. Rodgers, J. E. Mottershead, T. K. Hellen, J. Jarivis, R. Lohr, R. Howard-Hildige, A. Carlton and M. Whelan, "Material Properties From Small Specimens Using the Punch and Bulge Test", *Journal of Strain Analysis*, 1999, Vol. 34 No. 6.

[2] M. P., Manahan, A. S., Argon, and O. K., Harling, "The Development of a Miniaturized Disk Bend Test for the Determination of Post-irradiation Mechanical Properties", *Journal of Nuclear Material*, 1981, Vol. 103-104, 1545-1550.

[3] J. M. Baik, J. Kameda and O. Buck, "Small Punch Evaluation of Intergranular Embrittlement of an Alloy Steel", *Scr. Metall.*, 1983, Vol. 17, 1443-1447.

[4] C. H. Toh, Y. C. Shiau and S. Kobayashi, "Analysis of A Test Method of Sheet Metal Formability Using Finite-Element Method", *J. Eng. Industry*, Vol. 108, pp. 3-8, 1986.

[5] V. Hasek, "Untersuchung und theoretische beschreibung wichtiger einflusgrosen auf das Grenzfoman-derungsschaubild", *Institute of Metal Forming Report*, University of Stuttgart, West Germany, pp. 213-220, 1978.

[6] T. Yoshida, T. Katayama and M. Usuda, "Forming-Limit Analysis of Hemispherical-Punch Stretching Using the Three-Dimensional Finite-Element Method", *Journal of Material Processing Technology*, 1995.

[7] B. B. Yoon, R. S. Rao and N. Kikuchi, "Sheet Stretching: A Theoretical-Experimental Comparison", *Int. J. Mech. Sci.* Vol. 31, No. 8, pp. 579-590, 1989.

[8] K. H. Huebner, E. A. Thornton, and T. G. Byrom, *The Finite Element Method for Engineers*, 3rd edition, John Wiley & Sons Inc., 1995.

[9] P. Ludwik, *Elemente der Technologischen Mechanik*, Springer, Berlin, 1909.

[10] W. Ramberg and W. R. Osgood, "Description of Stress-Strain Curves by Three Parameters", *NACA Technical Note* No. 902, July 1943.

[11] R. G. Sauve and D. R. Metzger, "Advances in Dynamic Relaxation Techniques for Nonlinear Finite Element Analysis," *Journal of Pressure Vessel Technology*, Trans. ASME, Vol. 117, May 1995.

[12] W. K. Lee, D. R. Metzger, A. Donner, and O. E. Lepik, "The Use of A Small Punch Test Procedure to Determine Mechanical Properties", *Small Specimen Test Techniques, ASTM STP 1329*, W. R. Corwin, S. T. Rosinski, and E. van Walle, Eds., American Society for Testing and Materials, 1997.

[13] R. Courant, K. O. Friedrichs, and H. Lewy, "Uber die partiellen Differenzen-gleichungen der mathematischen Physik," *Math. Ann.*, Vol. 100, 1928, pp.32-74.

[14] G. E. Lucas, "A Review of Small Specimen Test Techniques for Irradiation Testing", *Metall. Trans. A*, 1990, Vol. 21, 1105-1119.

[15] R. D. Cook, D. S. Malkus, and M. E. Plesha, *Concept and Applications of Finite Element Analysis*, 3rd edition, John Wiley & Sons, 1989.

[16] G. E. Lucas, A. Okada, and M. Kiritani, "Parametric Analysis of the Disc Bend Test", *Journal of Nuclear Material*, 1986, Vol. 141-143, 532-535.

[17] L. E. Malvern, *Introduction to the Mechanics of a Continuous Medium*, Prentice Hall, Englewood Cliffs, New Jersey, 1969.

[18] J. Chakrabarty, *Theory of Plasticity*, McGraw-Hill Book Company, 1987.

[19] E. P. Popov, *Mechanics of Materials*, Prentice-Hall, New Jersey, 1976.

[20] Z. H. Zhong, *Finite Element Procedure for Contact-Impact Problems*, Oxford University Press, 1993.

[21] D. R. Metzger and R. G. Sauve, "Three-Dimensional Hourglass Stabilization for One Point Quadrature Finite Elements", Design Analysis, *Robust Methods and Stress Classification*, PVP Vol. 265, ASME, 1993.

[22] T. Belytschko, J. Ong, W. Liu, J. Kennedy, "Hourglass Control in Linear and Nonlinear Problems", *Computer Methods in Applied Mechanics and Engineering*, Vol. 43, pp 251-276, 1984.

[23] R. Viswanathan, "Small-Punch Testing for Assessing Thick-Section Components", *EPRI Journal*, January/February Issue, 1995, pp. 40-43.

[24] A. N. Sinclair, O. Lepik, M. Gabbani, B. Mukherjee, and E. Albertini, "Assessment of Fracture Toughness by a Punch Test with Miniature Specimens", Small Specimen Test Techniques Applied to Nuclear Reactor Thermal Annealing and Plant Life Extension, ASTM STP 1204, W. R. Corwin, F. M. Haggag, and W. L. Server, Eds., American Society for Testing and Materials, Philadelphia, 1992, pp. 162-181.

[25] R. G. Sauve and D. R. Metzger, "A Hybrid Explicit Solution Technique for Quasi-Static Transients", *Computer Technology: Applications and Methodology*, Vol. PVP-326, ASME, 1996.

[26] P. Underwood, "Dynamic Relaxation", *Computational Methods for Transient Analysis*, eds., T. Belytschko and T. J. R. Hughes, North Holland, Amsterdam, Vol. 1, 1983, pp. 245-265.

[27] T. Belytschko, "An Overview of Semidiscretization and Time Integration Procedures", *Computational Methods for Transient Analysis*, eds., T. Belytschko and T. J. R. Hughes, North Holland, Amsterdam, Vol. 1, 1983, pp. 1-66.

[28] K. J. Bathe, "On Finite Element Analysis of Large Deformation Frictional Contact Problems", Unification of Finite Element Methodds, Elsevier Science Publishers, B.V. 123, 1984.

[29] N. Chandrasekaran, W.E. Haisler, R.E. Goforth, "A Finite Element Solution Method for Contact Problems with Friction", *International Journal for Numerical Methods in Engineering*, Vol., 24, 477-495.

[30] R. G. Sauve, "A Contact-impact Algorithm for Three-dimensional Finite Deformation", Ontario Hydro Research Division Report, No., 90-314-K, 1990.

[31] R. F. Kulak, "Adaptive Contact Elements for Three-dimensional Explicit Transient Analysis", Comput. Meths. Appl. Mech. Engng., 72, 125-151, 1989.

[32] X. Mao and H. Takahashi, "Development of a Further-miniaturized Specimen of 3mm Diameter for TEM Disk Small Punch Tests", *Journal of Nuclear Materials*, Vol. 150, 1987, pp. 42-52.

[33] Y. H. Joo, T. Hashida and H. Takahashi, "Determination of Ductile-Brittle Transition Temperature (DBTT) in Dynamic small Punch Test", *Journal of Testing and Evaluation*, Vol. 20, No. 1, January 1992, pp. 6-14.

[34] J. R. Foulds, P. J. Woytowitz, T. Kim, and C. W. Jewett, "Fracture Toughness by Small Punch Testing", *Journal of Testing and Evaluation*, JTEVA, Vol. 23, No. 1, January 1995, pp. 3-10.

[35] W. Li, B. Rodgers, D. J. Brookfield, J. E. Mottershead, T. K. Hellen, R. Howard-Hildige, J. Jarvis, R. Lohr, A. Carlton and M. Whelan, "A Finite Element and Experimental Study of Punch and Bulge Testing", *Key Engineering Material*, Vol. 167-168, 1999, pp. 55-63.

[36] J. M. Manuel, B. Marques, P. A. F. Martins, "Three-Dimensional Finite Element Contact Algorithm for Metal Forming", *International Journal for Numerical Methods in Engineering*, Vol., 30, 1341-1354, 1990.

[37] T. Belytschko, M. O. Neal, "Contact-Impact by the Pinball Algorithm with Penalty and Lagrangian Methods", *International Journal for Numerical Methods in Engineering*, Vol., 31, 547-572, 1991.

[38] Jerry I. Lin, Ted Belytschko, "A Three-Dimensional Impact-Penetration Algorithm with Erosion", Computers and Structures, Vol., 25, No., 1, 95-104, 1987.

[39] K. J. Bathe, *Finite Element Procedure*, Prentice Hall, 1996

[40] Y. Shi, "A New Penalty Stiffness Treatment for Master-Slave Contact Surfaces", Mechanical Engineering Department, McMaster University, Hamilton, Ontario, Canada, September 2001.

[41] K. J. Bathe, *Finite Element Procedures in engineering Analysis*, Prentice-Hall, Englewood Cliffs, New Jersey, 1982.

[42] J. T. Oden, *Finite elements of Nonlinear Continua*, McGraw-Hill, 1972.

[43] O. C. Zienkiewicz and R. L. Taylor, *The Finite Element Method*, 4th Edition, McGraw-Hill, 1988.

[44] W. F. Hosford and R.M. Caddell, *Metal Forming — Mechanics and Metallurgy*, Prentice-Hall, 1983.

[45] I. H. Shames and C. L. Dym, *Energy and Finite element Methods in Structural Mechanics*, McGraw-Hill, 1985.

[46] R. G. Sauvé, "H3DMAP Version 6.0 - A General Three-Dimensional Finite Element Computer Code for Linear and Nonlinear Analysis of Structures", Ontario Power Technologies Report No. A-NSG-96-120, Rev. 1, 1999.

[47] Heber, "A Mixed Eulerian-lagrangian Displacement Model for Large Deformation Analysis in Solid Mechanics", Comp. Meth. Appl. Mech. Eng., 277/Vol., 43, 1984.

[48] S. C. Chapra, R. P. Canale, *Numerical Methods for Engineers*, 3rd edition, McGraw-Hill, 1998.

[49] O. C. Zienkiewicz, *The Finite Element Method*, 3rd edition, McGraw-Hill, London, 1997.

APPENDIX: Material Properties Determination by Empirical Expressions

A.1 Ludwik Fit

As the most popular stress-strain empirical equation, Ludwik's expression is used as the stress-strain relation for the least-squares regression. Chapter 1 gives the expression as

$$\sigma = \sigma_y + H\varepsilon^n \tag{A-1}$$

where σ_y is the yield stress, H is the hardening rate and exponent $n = 0,1$.

The internal strain energy from the finite element model for all elements can be expressed as

$$U^{fe} = \sum_{i=1}^{ne} V_i \left(\sigma_y \varepsilon_i + H \frac{\varepsilon_i^{n+1}}{n+1} \right) \tag{A-2}$$

The sum of the squares of the residual errors over time period t between the measured and model strain energy is given as

$$S_r = \sum_j^{npt}\left[U^m(t_j) - \sum_i^{ne} V_i\left(\sigma_y \varepsilon_i(t_j) + H\frac{\varepsilon_i^{n+1}(t_j)}{n+1}\right)\right]^2 \tag{A-3}$$

To make Eq. (A-3) easy for solving the curve fitting parameters, exponent n was considered as a constant looped over the range from 0 to 1 with a small increment (say 1/30). Eq. (A-3) then becomes a linear equation, and only two parameters are left for solving.

To determine the values for σ_y and H, set the derivatives of Eq. (A-3) with respect to yield stress and hardening rate equal to zero respectively:

$$\frac{\partial S_r}{\partial \sigma_y} = 0, \qquad \frac{\partial S_r}{\partial H} = 0 \tag{A-4}$$

From $\dfrac{\partial S_r}{\partial \sigma_y} = 0$

$$\begin{aligned}\sum_j\left(U^m(t_j)\sum_k V_k\,\varepsilon_k(t_j)\right) - \sigma_y\left[\sum_j\left(\sum_i V_i\,\varepsilon_i(t_j)\sum_k V_k\,\varepsilon_k(t_j)\right)\right] \\ - H\left[\sum_j\left(\sum_i V_i\,\frac{\varepsilon_i^{n+1}(t_j)}{n+1}\right)\left(\sum_k V_k\,\varepsilon_k(t_j)\right)\right] = 0\end{aligned} \tag{A-5}$$

Eq. (A-5) can be simplified as

$$B\sigma_y + CH = A \tag{A-6}$$

where A, B and C are known coefficients of the equation and expressed as

$$A = \sum_j \left(U^m(t_j) \sum_k V_k \, \varepsilon_k(t_j) \right)$$

$$B = \left[\sum_j \left(\sum_i V_i \, \varepsilon_i(t_j) \sum_k V_k \, \varepsilon_k(t_j) \right) \right]$$

$$C = \left[\sum_j \left(\sum_i V_i \, \frac{\varepsilon_i^{n+1}(t_j)}{n+1} \right) \left(\sum_k V_k \, \varepsilon_k(t_j) \right) \right] \qquad \text{(A-7)}$$

From $\frac{\partial S_r}{\partial H} = 0$

$$\sum_j \left(U^m(t_j) \sum_k V_k \, \frac{\varepsilon_k^{n+1}(t_j)}{n+1} \right) - \sigma_y \left[\sum_j \left(\sum_i V_i \, \varepsilon_i(t_j) \sum_k V_k \, \frac{\varepsilon_k^{n+1}(t_j)}{n+1} \right) \right] - H \left[\sum_j \left(\sum_i V_i \, \frac{\varepsilon_i^{n+1}(t_j)}{n+1} \right) \left(\sum_k V_k \, \frac{\varepsilon_k^{n+1}(t_j)}{n+1} \right) \right] = 0 \qquad \text{(A-8)}$$

Eq. (A-8) can be simplified as

$$E\sigma_y + FH = D \qquad \text{(A-9)}$$

where D, E and F are known coefficients of the equation and expressed as

$$D = \sum_j \left(U^m(t_j) \sum_k V_k \, \frac{\varepsilon_k^{n+1}(t_j)}{n+1} \right)$$

$$E = \left[\sum_j \left(\sum_i V_i \, \varepsilon_i (t_j) \sum_k V_k \, \frac{\varepsilon_k^{n+1}(t_j)}{n+1} \right) \right]$$

$$F = \left[\sum_j \left(\sum_i V_i \, \frac{\varepsilon_i^{n+1}(t_j)}{n+1} \right) \left(\sum_k V_k \, \frac{\varepsilon_k^{n+1}(t_j)}{n+1} \right) \right] \qquad \text{(A-10)}$$

Combined Eq. (A-6) and Eq. (A-9), the yield stress and hardening rate can be solved as

$$\sigma_y = \frac{AF - CD}{BF - CE}, \qquad H = \frac{DB - AE}{BF - CE} \qquad \text{(A-11)}$$

A.2 Ramberg-Osgood Fit

Ramberg-Osgood equation is another frequently used empirical material property expression. Chapter 1 gives its form as

$$\varepsilon = \frac{\sigma}{E} \left\{ 1 + \alpha \left(\frac{\sigma}{\sigma_0} \right)^{m-1} \right\} \qquad \text{(A-12)}$$

where σ_0 is a nominal yield stress, α and m are dimensionless constant, $m \geq 1$.

Since the elastic strain ε_e can be expressed as

$$\varepsilon_e = \frac{\sigma}{E} \qquad \text{(A-13)}$$

Equation A-12 becomes

$$\varepsilon - \varepsilon_e = \frac{\alpha\sigma_0}{E}\left(\frac{\sigma}{\sigma_0}\right)^m = \varepsilon_p \qquad \text{(A-14)}$$

where ε_p is the plastic strain.

Rearrange the equation A-14, we get

$$\sigma = \sigma_0\left(\frac{E}{\alpha\sigma_0}\right)^n \varepsilon_p^n \qquad \text{(A-15)}$$

where exponent n is the inverse of m and $n = 0{,}1$.

Equation A-15 is a special form of Ludwik equation with the yield stress $\sigma_y = 0$ and omitting the elastic strain. Using the same Ludwik fit algorithm and setting the yield stress coefficient σ_y to zero, the coefficient of Eq. A-15 can be obtained.